İÇİNDEKİLER (CONTENTS)

Özel Sayı Makalesi (Special Issue Article)

DESIGN OF VISCO-ELASTIC SUPPORTS FOR TIMOSHENKO CANTILEVER BEAMS

[1] Ersin AYDIN [iD] , [2,*] Yunus Emre KEBELİ [iD] [3] Hüseyin ÇETİN [iD] , [4] Baki ÖZTÜRK [iD]

[1,2]Niğde Ömer Halisdemir University, Engineering Faculty, Civil Engineering Department, Niğde, TURKIYE
[3]Niğde Ömer Halisdemir University, Technical Sciences Vocational School, Contruction Technologies, Niğde, TÜRKİYE
[4]Hacettepe University, Engineering Faculty, Civil Engineering Department, Ankara, TURKIYE
[1] eaydin@ohu.edu.tr, [2] yunusemrekebeli@ohu.edu.tr, [3] hcetin@ohu.edu.tr, [4] bakiozturk@hacettepe.edu.tr

Highlights

- This study investigates the most suitable support configuration for a cantilever beam, including viscoelastic supports across different vibration modes.

- The determination of the ideal stiffness and damping coefficients of the viscoelastic components is achieved by minimizing the absolute acceleration at the free end of the beam.

- Analytical derivative equations are formulated for both the stiffness and damping parameters.

- The present work introduces a concurrent optimization approach for both stiffness and damping.

- The effectiveness of viscoelastic supports in predicting ideal spring and damping coefficients and their ability to provide optimal support solutions for various vibration modes are demonstrated.

*Corresponding Author: Yunus Emre KEBELİ, yunusemrekebeli@ohu.edu.tr

DESIGN OF VISCO-ELASTIC SUPPORTS FOR TIMOSHENKO CANTILEVER BEAMS

¹ Ersin AYDIN , **²,* Yunus Emre KEBELİ** **³ Hüseyin ÇETİN** , **⁴ Baki ÖZTÜRK**

¹,²Niğde Ömer Halisdemir University, Engineering Faculty, Civil Engineering Department, Niğde, TÜRKİYE
³Niğde Ömer Halisdemir University, Technical Sciences Vocational School, Contruction Technologies, Niğde, TÜRKİYE
⁴Hacettepe University, Engineering Faculty, Civil Engineering Department, Ankara, TÜRKİYE
¹ eaydin@ohu.edu.tr, ² yunusemrekebeli@ohu.edu.tr, ³ hcetin@ohu.edu.tr, ⁴ bakiozturk@hacettepe.edu.tr

ABSTRACT: The appropriate design of supports, upon which beams are usually placed as structural components in many engineering scenarios, has substantial significance in terms of both structural efficacy and cost factors. When beams experience various dynamic vibration effects, it is crucial to contemplate appropriate support systems that will effectively adapt to these vibrations. The present work investigates the most suitable support configuration for a cantilever beam, including viscoelastic supports across different vibration modes. Within this particular framework, a cantilever beam is simulated using beam finite elements. The beam is positioned on viscoelastic supports, which are represented by simple springs and damping elements. These supports are then included in the overall structural model. The equation of motion for the beam is first formulated in the temporal domain and then converted to the frequency domain via the use of the Fourier Transform. The basic equations used in the frequency domain are utilized to establish the dynamic characteristics of the beam by means of transfer functions. The determination of the ideal stiffness and damping coefficients of the viscoelastic components is achieved by minimizing the absolute acceleration at the free end of the beam. In order to minimize the objective function associated with acceleration, the nonlinear equations derived from Lagrange multipliers are solved using a gradient-based technique. The governing equations of the approach need partial derivatives with respect to design variables. Consequently, analytical derivative equations are formulated for both the stiffness and damping parameters. The present work introduces a concurrent optimization approach for both stiffness and damping. Passive constraints are established inside the optimization problem to impose restrictions on the lower and higher boundaries of the stiffness and damping coefficients. On the other hand, active constraints are used to ascertain the specific values of the overall stiffness and damping coefficients. The efficacy of the established approach in estimating the ideal spring and damping coefficients of viscoelastic supports and its ability to provide optimal support solutions for various vibration modes have been shown via comparative experiments with prior research.

Keywords: Timoshenko beam, Transfer function, Visco-elastic support, Beam vibration, Damping, Spring

1. INTRODUCTION

The support and bond conditions of beams, which are frequently employed in engineering problems, are crucial to their dynamic behavior. It can be observed in all areas of structural engineering design, in building-type structures during construction, and in welded or riveted machine element connections in marine and aircraft structures. Support conditions play a significant role in structure analysis for more realistic problem resolution. Changes in support positions and conditions can also substantially alter structural performance. It must be designed with attention. Not only are bearings anticipated to secure the structure, but they can also be redesigned to enhance structural performance. Unexplored is the optimization of support locations to reduce structural displacements. Timoshenko et al. [1] studied the unconstrained vibration of beams resting on variable Winkler spring foundations. Wei and Yida [2]

examined the dynamic response of a viscoelastic Winkler foundation supported elastic beam. Chung et al. [3] proposed an analytical method for determining the natural frequencies of beams that are supported elastically at both extremities and constrained in the middle. Chen and Sheu [4] investigated a damped laminated Timoshenko beam axially laid on a viscoelastic base. [5] Metrikine and Dieterman studied the uniform motion of a mass along an axially compressed Euler-Bernoulli beam on a viscoelastic base. Using the Winkler model, Lee et al. [6] investigated the spontaneous vibrations of piles partially driven into elastic soil. The effect of point visco-elastic supports on the dynamic stability of visco-elastic piles was investigated by Zhen-Yu et al. [7]. Chen and Huang investigated the Timoshenko beam on a viscoelastic Winkler foundation for a range of beam, foundation, and loading conditions. Chen et al. examined the response of the Timoshenko beam on a viscoelastic base to a moving harmonic load [8,9]. Ansari et al. [10] investigated the inside-outside resonance vibration of a finite Euler-Bernoulli beam supported by a nonlinear viscoelastic base through which a moving load passes. Zhen et al. [11] studied the steady-state responses of an infinite Euler-Bernoulli beam supported by a nonlinear viscoelastic Winkler foundation and subjected to a harmonic moving load. Zheng et al. examined the instability analysis of a beam resting on a visco-elastic foundation and subjected to a moving mass-spring-damping system [12]. Vostroukhov and Metrikine [13] conducted a theoretical investigation into the steady-state dynamic response of a train traveling on a railway track supported by periodically placed viscoelastic supports. Metrikine examined the steady-state condition of an infinite spring on a nonlinear viscoelastic base subjected to a moving point load [14]. [15] Majorana and Pomaro investigated the dynamic stability of an elastic beam supported by viscoelastic translational and rotational supports. Basu and Rao devised analytical solutions for the steady-state response of an infinite beam resting on a viscoelastic foundation and subjected to a constant-speed concentrated load [16]. Froio and co. [17] They obtained numerically the Discontinuous Least Squares Finite Element Method formulation for the steady-state response of a tensioned spring on viscoelastic support under live load using the Discontinuous Least Squares Finite Element Method. Dimitrovová [18] investigated the dynamic interaction between two near masses on a Pasternak beam in a viscoelastic soil.

The optimal location of beam supports for elastic and plastic behaviour has been researched [19-21]. Akesson and Olhoff examined the minimum rigidity configuration that maximizes the fundamental natural frequency [22]. Hou and Chuang [23] determined the optimal support condition for a cantilever beam by deriving the sensitivity of the natural frequency to the support position. Wang derived the variation of frequency based on the support position in closed form for an Euler-Bernolli beam utilizing the conventional normal modal method [24]. In a separate study, Wang and Chen [25] used a genetic algorithm to determine the optimal beam support positions for various boundary conditions. Won and Park demonstrated the optimal location of a beam's supports based on the rigidity of the supports [26]. Aristizabal analyzed the free vibration of non-prismatic beams and columns and proposed a matrix method solution [27]. Sinha and Friswell formulated the location of the spring support and the global stiffness matrix in a beam element using element shape functions [28]. Aydin determined the optimal elastic support rigidity and location to minimize the end displacement or acceleration of a cantilever beam subjected to structural natural vibration. They solved the problem of optimizing the support conditions of stiffnesses and positions to minimize the shear force of a beam during various harmonic vibrations. Aydin et al. [29-31] investigated the determination of optimal elastic springs for cantilever beams supported by elastic foundations. Wang and Wen investigated the optimal position of viscoelastic supports for dampening beam vibration under harmonic load [32].

Certain researchers have investigated the optimization of column supports that maximize fracture load [33-35]. Lee and Co. Solutions were shown to find the free vibrations of beams for general boundary conditions and a new method was devised to find the buckling loads and natural harmonics of prismatic beams supported by an elastic spring at their center [36].

Huang and Huang [37] utilized the Laplace transform method to analyze the response and mechanical properties of viscoelastic Timoshenko beams. Liu et al. [38] derived closed form frequency sensitivities using the Lagrange Multipliers method based on the Rayleigh principle. Takewaki [39] presented a

method using transfer functions to optimize the location and number of dampers in a built-up beam resting on viscous dampers. Sun analyzed the displacement of the beam on a viscoelastic base subjected to moving masses [40] using Green's function and Fourier transform in closed form. Kargarnovin et al. [41] studied the response of beams supported by nonlinear viscoelastic foundations to harmonic live loads. Çalım [42] analyzed the dynamic behavior of Pasternak-type beams subjected to time-dependent stresses on viscoelastic foundations. Mazilu [43] discussed the response of an infinite cable on viscoelastic support subjected to a moving harmonic load using the Green function method. Abdelghany et al. [44] investigated the dynamic response of a non-uniform beam subjected to a live load and supported by a non-linear viscoelastic foundation. Using integral transformation and contour integral methods, Dimitrovová [45] studied the dynamic response of an infinite beam resting on a classical Pasternak foundation and subjected to a moving mass, taking into consideration inhomogeneous initial conditions. Roy et al. [46] examined the interaction between an infinite spring supported by a homogeneous viscoelastic layer and a series of discrete mechanical systems all moving at the same constant speed. Dimitrovová developed a new semi-analytical solution for a mass moving uniformly on a beam, assuming homogeneous initial conditions, on a two-parameter visco-elastic basis. In another study [47, 48], Dimitrovová obtained a semi-analytical solution for a uniformly moving mass on a beam supported by a viscoelastic foundation with two parameters. Huang and Zou [49] studied the dynamic response of an elastic circular plate on a half-field viscoelastic Winkler foundation influenced by a moving rigid body with a decreased initial velocity. Aydin et al. modelled a Timoshenko-type cantilever beam resting on viscoelastic supports with finite elements, applied the Fourier transform to the equation of motion, derived governing equations in the frequency space, and demonstrated how they should be supported for minimum vibration behaviour with the displacement transfer function [50]. Cimellaro derived it to locate the optimal positioning of viscoelastic dampers using the transfer function vector of the absolute acceleration at any shear structure's natural frequency. The absolute acceleration transfer function vector is expressed for a cantilever beam supported by elastic springs [51].

This research aimed to evaluate the optimization of spring and damper positions and amounts with the objective of minimizing the amplitude of the transfer function for top absolute acceleration. The Fourier Transform was utilized to analyze the equation of motion represented in the time domain, enabling the expression of its behavior via transfer functions. The optimization issue is formally described using the Lagrange Multipliers technique, and the optimality criteria are then determined. The sensitivity equations are obtained by analytical derivation. Takewaki [39] has updated the Steepest Direction Search Algorithm (SDSA) approach to address the challenge of optimizing damper performance. This adaptation involves considering both optimal damping and stiffness distribution. The efficacy of the suggested strategy is shown via the presentation of a numerical example. The suggested approach involves doing frequency domain computations and temporal domain analysis to effectively reduce the vibration of the beam.

2. FORMULATION OF THE PROBLEM OF CANTILEVER BEAM SITTING ON VISCO-ELASTIC SUPPORTS

A cantilever beam resting on springs and viscous dampers, defined as visco-elastic supports, is seen in Figure 1 below. Here k_n and c_n are the stiffness and damping coefficients of the visco-elastic support at the nth node. Considering that the cantilever beam is divided into n frame elements and a lumped mass is added to its end point, the equation of motion of a Timoshenko type cantilever beam in the absence of visco-elastic supports with 2n degrees of freedom is expressed as

$$M\ddot{u}(t) + C\dot{u}(t) + Ku(t) = -Mr\ddot{u}_g(t) \tag{1}$$

In this equation, $u(t)$ is displacement, $\dot{u}(t)$ is velocity and $\ddot{u}(t)$ is acceleration; M, C and K show the mass, damping and stiffness matrix of the beam. r refers to the influence vector whose elements showing

the direction of ground motion are one, and $\ddot{u}_g(t)$ refers to the acceleration of the vertical support movement.
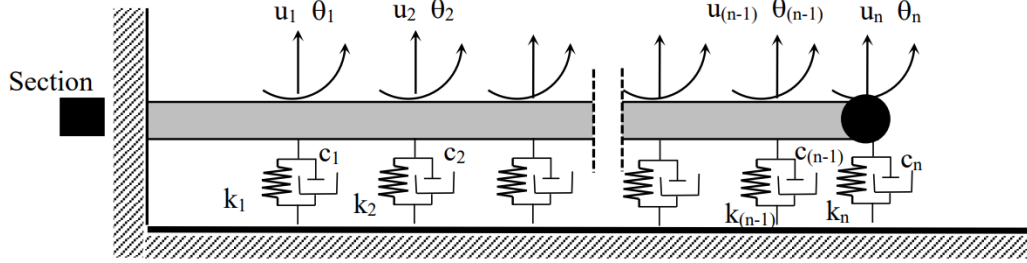
Figure 1. Cantilever beam resting on visco-elastic supports

If Fourier Transform is applied to Equation (1), $U(\omega)$ and $\ddot{U}_g(\omega)$; Provided that $u(t)$ and $\ddot{u}_g(t)$ are Fourier transforms, Equation (1) becomes the following:

$$(K + i\omega C - \omega^2 M)U(\omega) = -Mr\ddot{U}_g(\omega) \tag{2}$$

Here, ω refers to the circular frequency of the external effect, and i refers to $\sqrt{-1}$. As seen in Figure 1, when the beam is supported from below with visco-elastic supports, Equation (2)

$$\left((K + K_{ad}) + i\omega(C + C_{ad}) - \omega^2 M\right)U_{ad}(\omega) = -Mr\ddot{U}_g(\omega) \tag{3}$$

Here, K_{ad} and C_{ad} denote additional stiffness and damping matrices with terms belonging to visco-elastic supports. $U_{ad}(\omega)$ expresses the Fourier transform of the displacements after the springs are added. As a new parameter,

$$\hat{U}(\omega) = \frac{U_{ad}(\omega)}{\ddot{U}_g(\omega)} \tag{4}$$

A transfer function can be defined as [39]. Here, if the frequency value is taken as equal to the frequency corresponding to the nth mode behavior of the beam ($\omega = \omega_n n$), the support movement will be defined as a harmonic movement with frequency ω_n. Using Equation (4), Equation (3) is rearranged as follows:

$$A\hat{U}(\omega_n) = -Mr \tag{5}$$

Here $\hat{U}(\omega_n)$ refers to the transfer function of the displacements calculated at the nth natural frequency of the structure. Matrix A, which contains the spring stiffness coefficients ($k_1, k_2, ..., k_n$) and damping coefficients ($C_1, C_2, ..., C_n$) which are design variables can be written as.

$$A = (K + K_{ad}) + i\omega_n(C + C_{ad}) - \omega_n^2 M \tag{6}$$

In this equation, K, M and C matrices are known. The coefficients in the K_{ad} and C_{ad} matrices containing the design variables will be found to be optimum. If equation (5) is rewritten as follows:

$$\widehat{U}(\omega_n) = -A^{-1}Mr \tag{7}$$

The transfer function of absolute acceleration is found for the nth mode. The transfer function for the absolute acceleration given below was derived by Cimellaro [51] and was used in this study to solve the problem of a cantilever beam resting on a visco-elastic foundation.

$$\widehat{\ddot{U}}(\omega_n) = \psi(\omega_n) = -M^{-1}\big(K + K_{ad} + i\omega_n(C + C_{ad})\big)\widehat{U} \tag{8}$$

2.1. Optimization Problem of Visco-Elastic Supports

While making optimum designs of structures or building elements, many different objective functions and constraints are defined depending on the problem. Weight, frequency, buckling load, specific displacements, accelerations, energy, etc. of the structural system. Quantities such as these can sometimes appear as objective functions in minimization and sometimes maximization problems. Apart from these, many objective functions can also be considered. The objective function appropriate to the nature of the problem can be selected by the designer. In this study, the transfer function amplitude of the end absolute acceleration of the beam was selected as the objective function for the optimization of visco-elastic supports supporting a built-in beam. Mathematical representation of the objective function used can be written in the form.

$$Min \quad f(K_{ad}, C_{ad}) = f(k_1, k_2, k_3, \ldots, k_n, c_1, c_2, c_3, \ldots, c_n) \tag{9}$$

Here, f the aim function is defined as the amplitude of the transfer function of the end absolute acceleration of the beam.

$$f(K_{ad}, C_{ad}) = |\psi(\omega_n)| \qquad (i = 1, 2, \ldots, n) \tag{10}$$

Here $|\psi(\omega_n)|$ expresses the absolute value of the transfer function amplitude of the vertical acceleration at the end point of the beam. Additionally, for each spring and damping coefficient,

$$0 \leq k_i \leq \bar{k}_i \qquad (i = 1, 2, \ldots, n) \tag{11}$$
$$0 \leq c_i \leq \bar{c}_i \qquad (i = 1, 2, \ldots, n) \tag{12}$$

Passive restrictions can be given in this form. Here $\bar{k}_i$ indicates the upper limit of the spring coefficient and $\bar{c}_i$ indicates the upper limit of the damping coefficient. There is also an active restriction on the sum of the spring and damping coefficients. These can be written as

$$\sum_{i=1}^{n} k_i = \bar{K} \tag{13}$$
$$\sum_{i=1}^{n} c_i = \bar{C} \tag{14}$$

Here, $\bar{K}$ and $\bar{C}$ represent the sum of the spring and damping coefficients to be added.

2.2. Optimality Criteria

A gradient-based optimization approach is used here. Optimality criteria can be derived using the Lagrange Multipliers method. Depending on the generalized Lagrangian functional objective function, constraint functions and Lagrange multipliers (λ, μ and ν) can be written as

$$L(k_i, c_i, \lambda, \mu_i, \nu_i, \alpha_i, \beta_i) = f(k_i, c_i) + \lambda_1 \left(\sum_{i=1}^{n} (k_i - \bar{K}) \right) + \lambda_2 \left(\sum_{i=1}^{n} (c_i - \bar{C}) \right)$$
$$+ \sum_{i=1}^{n} \mu_i (0 - k_i) + \sum_{i=1}^{N} \nu_i (k_i - \bar{k}_i) + \sum_{i=1}^{n} \alpha_i (0 - c_i) + \sum_{i=1}^{N} \beta_i (c_i - \bar{c}_i) \tag{15}$$

If Equation (15) is differentiated according to the design variables (k_i and c_i) and Lagrange Multipliers,

$$\frac{\partial f}{\partial k_i} + \lambda_1 = 0 \ (i = 1,2, \dots, n) \ \ 0 < k_i < \bar{k}_i \tag{16}$$

$$\sum_{i=1}^{N} k_i - \bar{K} = 0 \tag{17}$$

$$\frac{\partial f}{\partial c_i} + \lambda_2 = 0 \ (i = 1,2, \dots, n) \ \ 0 < c_i < \bar{c}_i \tag{18}$$

$$\sum_{i=1}^{N} c_i - \bar{C} = 0 \tag{19}$$

Optimality criteria are derived as follows. Here, $\frac{\partial f}{\partial k_i}$ and $\frac{\partial f}{\partial c_i}$ express the partial derivative of the objective function with respect to the ith design variable k_i and c_i. For lower and upper constraints, Equation (16) and Equation (18) can be changed and written as follows:

$$\frac{\partial f}{\partial k_i} + \lambda \geq 0 \qquad k_i = 0 \tag{20}$$

$$\frac{\partial f}{\partial k_i} + \lambda \leq 0 \qquad k_i = \bar{k}_i \tag{21}$$

$$\frac{\partial f}{\partial c_i} + \lambda \geq 0 \qquad c_i = 0 \tag{22}$$

$$\frac{\partial f}{\partial c_i} + \lambda \leq 0 \qquad c_i = \bar{c}_i \tag{23}$$

These equations can be solved with a modified version of SDSA given by Takewaki [39].

2.2. Solution Algorithm

If the partial derivative of Equation (5) is taken according to the design variables,

$$\frac{\partial A}{\partial k_j} \widehat{U} + A \frac{\partial \widehat{U}}{\partial k_j} = 0 \qquad (j = 1 \dots, n) \tag{24}$$

$$\frac{\partial A}{\partial c_j} \widehat{U} + A \frac{\partial \widehat{U}}{\partial c_j} = 0 \qquad (j = 1 \dots, n) \tag{25}$$

Equations (24) and (25) derived by Takewaki [39]. The first order derivatives of absolute accelerations in Equation (8) were derived by Cimellaro and can be written as follows [51].

$$\frac{\partial \psi}{\partial k_j} = -A^{-1} \frac{\partial A}{\partial k_j} \omega_s^2 \widehat{U} \tag{26}$$

$$\frac{\partial \psi}{\partial c_j} = -A^{-1} \frac{\partial A}{\partial c_j} \omega_s^2 \widehat{U} \tag{27}$$

Transfer function values of the forces in Equation (5),

$$\psi_i = Re[\psi_i] + Im[\psi_i] \tag{28}$$

It is expressed in complex form. Each of the derived terms calculated from Equations (26)-(27) can also be shown as follows:

$$\frac{\partial \psi_i}{\partial k_j} = Re\left[\frac{\partial \psi_i}{\partial k_j}\right] + Im[\frac{\partial \psi_i}{\partial k_j}] \tag{29}$$

$$\frac{\partial \psi_i}{\partial c_j} = Re\left[\frac{\partial \psi_i}{\partial c_j}\right] + Im[\frac{\partial \psi_i}{\partial c_j}] \tag{30}$$

If the absolute value of ψ_i, which is the acceleration, is written as follows, it can be calculated as:

$$|\psi_i| = \sqrt{(Re[\psi_i])^2 + (Im[\psi_i])^2} \tag{31}$$

If the derivative of Equation (31) is taken with respect to the jth design variable (k_i and c_i),

$$\frac{\partial |\psi_i|}{\partial k_j} = \frac{1}{|\psi_i|} \left\{ Re[\psi_i]\left(Re\left[\frac{\partial \psi_i}{\partial k_j}\right]\right) + Im[\psi_i]\left(Im\left[\frac{\partial \psi_i}{\partial k_j}\right]\right) \right\} \tag{32}$$

$$\frac{\partial |\psi_i|}{\partial c_j} = \frac{1}{|\psi_i|} \left\{ Re[\psi_i]\left(Re\left[\frac{\partial \psi_i}{\partial c_j}\right]\right) + Im[\psi_i]\left(Im\left[\frac{\partial \psi_i}{\partial c_j}\right]\right) \right\} \tag{33}$$

In this way, the first order partial derivative of the objective function with respect to the jth design variable is found.

Solution Algorithm ($k_i \leq \bar{k}_i$ and $c_i \leq \bar{c}_i$):
Step1. Initially, take all the stiffness and damping coefficients of the visco-elastic supports as $k_i = 0$ and $c_i = 0$ ($j = 1,2, \dots, n$). Assume the total stiffness and damping coefficient to be added in each step as $\Delta K = \frac{\bar{K}}{m}$ and $\Delta C = \frac{\bar{C}}{m}$ and choose the number of design steps (m).
Step2. Calculate $\frac{\partial f}{\partial k_j}$ and $\frac{\partial f}{\partial c_j}$ using Equations (29)-(30).

Step3. Find the indices p and r, satisfying the conditions $-\frac{\partial f}{\partial k_p} = Max(-\frac{\partial f}{\partial k_j})$ and $-\frac{\partial f}{\partial c_r} = Max(-\frac{\partial f}{\partial c_j})$.

Step4. Renew the objective function f as $f + \frac{\partial f}{\partial k_p}\Delta k_p + \frac{\partial f}{\partial c_r}\Delta c_r$, where $\Delta k_p = \Delta K$ and $\Delta c_r = \Delta C$. Δk_p and Δc_r are the amount of stiffness and damping coefficient to be added in that design step.

Step5. Repeat Step2 through Step5 until the constraints $\sum_{i=1}^{n} k_i = \overline{K}$ and $\sum_{i=1}^{n} c_i = \overline{C}$ are satisfied.

In this algorithm, the method intended by Takewaki [39] to find optimum damping coefficients is reduced to a state where only first-order derivatives are used. In order to apply the solution algorithm, the derivative of matrix A must be found according to the design variables (k_i) indicating stiffness.

Formulation of the eigenvalue-eigenvector problem in a vibrating mechanical system can be expressed as:

$$\boldsymbol{K_T}(k)\boldsymbol{\Phi_n} = \Omega_n(k)\mathbf{M\Phi_n} \tag{34}$$

It can be specified as $\boldsymbol{K_T} = (\boldsymbol{K} + \boldsymbol{K_{ad}})$. Here $\Omega_n = \omega_n^2$ and $\boldsymbol{\Phi_n}$ is n for the undamped state. Shows eigenvalues and eigenvectors. If equation (34) is multiplied by $\boldsymbol{\Phi_n}^T$ from the left, the following equation is obtained.

$$\boldsymbol{\Phi_n^T}\mathbf{K_T}(k)\boldsymbol{\Phi_n} = \Omega_n(k)\boldsymbol{\Phi_n^T}\mathbf{M\Phi_n} \tag{35}$$

Here $\overline{m}_n = \boldsymbol{\Phi_n^T}\mathbf{M\Phi_n}$ is the modal mass for the nth mode and $\overline{k}_n = \boldsymbol{\Phi_n^T}\mathbf{K_T\Phi_n}$. If it is defined as modal stiffness for this mode and $\Omega_n(k)$ is written from Equation (35) is obtained as.

$$\Omega_n(k) = \frac{\overline{k}_n}{\overline{m}_n} \tag{36}$$

The first order derivative of $\Omega_n(k)$ according to the design variable for the jth stiffness is found as follows.

$$\frac{\partial \Omega_n}{\partial k_j} = \frac{1}{\overline{m}_n}\frac{\partial \overline{k}_n}{\partial k_j} \tag{37}$$

Here $\frac{\partial \overline{k}_n}{\partial k_j} = \boldsymbol{\Phi_n^T}\frac{\partial K_T}{\partial k_j}\boldsymbol{\Phi_n}$ is calculated with the help of the equation. If $\Omega_n = \omega_n^2$ is added into Equation (37) and arranged,

$$\frac{\partial \omega_n}{\partial k_j} = \frac{1}{2\overline{m}_n\omega_n}\frac{\partial \overline{k}_n}{\partial k_j} \tag{38}$$

In this form, the first order derivative of the nth undamped natural frequency with respect to the jth stiffness coefficient is found. The structural damping matrix can be written as follows, proportional to the mass can be written as.

$$\boldsymbol{C} = \alpha(k)\boldsymbol{M} \tag{39}$$
$$\alpha(k) = 2\zeta\omega_n(k) \tag{40}$$

If Equation (40) is placed into Equation (39) and its derivative is taken according to the jth stiffness coefficient, the first order derivative of the structural damping matrix according to the design variable can be found as follows:

$$\frac{\partial \boldsymbol{C}}{\partial k_j} = 2\zeta \frac{\partial \omega_n}{\partial k_j} \mathbf{M} \tag{41}$$

Derivative of matrix A given by Equation (6) according to the jth stiffness design variable is found as.

$$\frac{\partial \boldsymbol{A}}{\partial k_j} = \frac{\partial \boldsymbol{K_T}}{\partial k_j} + i \frac{\partial \omega_n}{\partial k_j} (\boldsymbol{C} + \boldsymbol{C_{ad}}) + i\omega_n \frac{\partial (\boldsymbol{C} + \boldsymbol{C_{ad}})}{\partial k_j} \\ - \frac{\partial \Omega}{\partial k_j} \boldsymbol{M} \tag{42}$$

2.3. Example Problem

The cantilever beam seen in Figure 2 has 6 m space and is divided into 1 m finite element parts. There are six nodes in total. A linear and an angular displacement were assumed at each node and modeled as a Timoshenko beam. Density of the beam material ρ=7.8 10^3 kg/m³, modulus of elasticity E=2.06 10^{11} N/m², shear modulus G=7.94 10^{10} N/m², correction factor κ=5/6, cross-sectional area A=0.05 m², moment of inertia I= 2.08 10^{-4} m⁴ and the total stiffness amount, $\overline{K}$, and the total damping coefficient amount, $\overline{C}$ are selected separately for the first three modes as in Table 1 below. $\Delta C = \overline{C}/300$ and $\Delta C = \overline{C}/300$. Additionally, a 100 kg mass was added to the end of the beam.
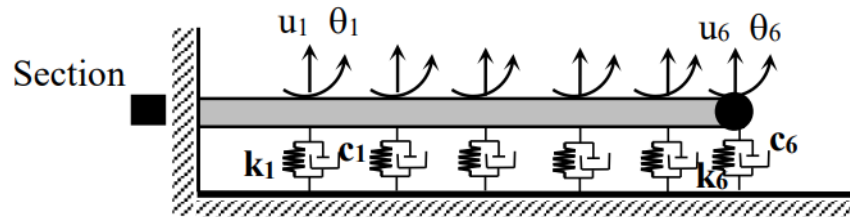
Figure 2. 12 degrees of freedom cantilever beam resting on visco-elastic supports

Table 1. Total stiffness and total damping amounts taken according to modes in the model

Modes	$\overline{K}$ (N/m)	$\overline{C}$ (Ns/m)
1st mode	8.0 10^5	6.0 10^3
2nd mode	1.0 10^7	6.0 10^4
3rd mode	5.0 10^7	12.0 10^4

In the solutions for the first three modes, Aydin et al. [50] considered displacement control in a previous study to obtain optimum design, and this study, which is considered acceleration control, is compared with this Figure 3 shows the mode shapes of the cantilever beam with and without optimum visco-elastic support.
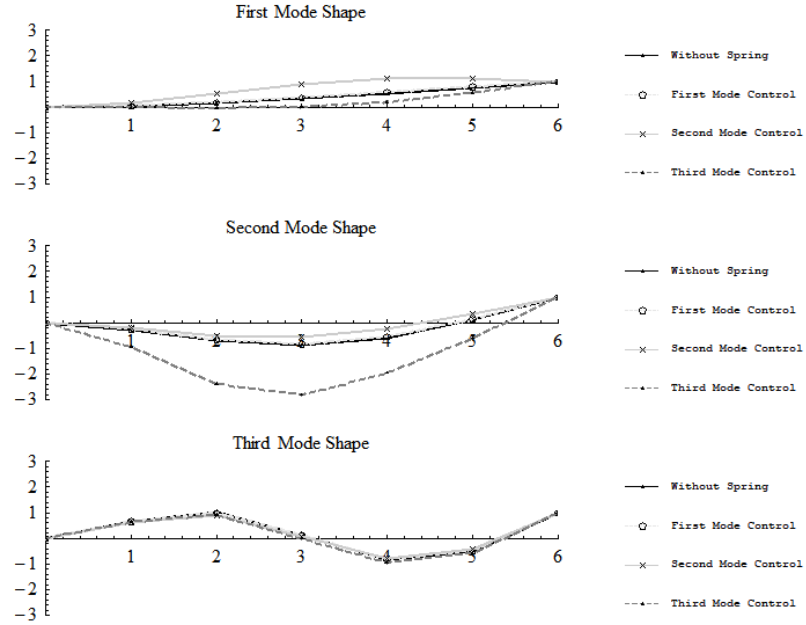
Figure 3. The first three mode shapes of the beam according to without both visco-elastic supports and optimal supports.

2.3.1 According to the first mode

To apply the optimization algorithm explained in the subject, $\omega = \omega_1$ was first selected, the selected total stiffness amount ($\bar{K} = 8.0 \ 10^5 \ N/m$) and the total damping amount ($\bar{C} = 6.0 \ 10^3 \ Ns/m$). is placed optimally according to the first mode of the structure.
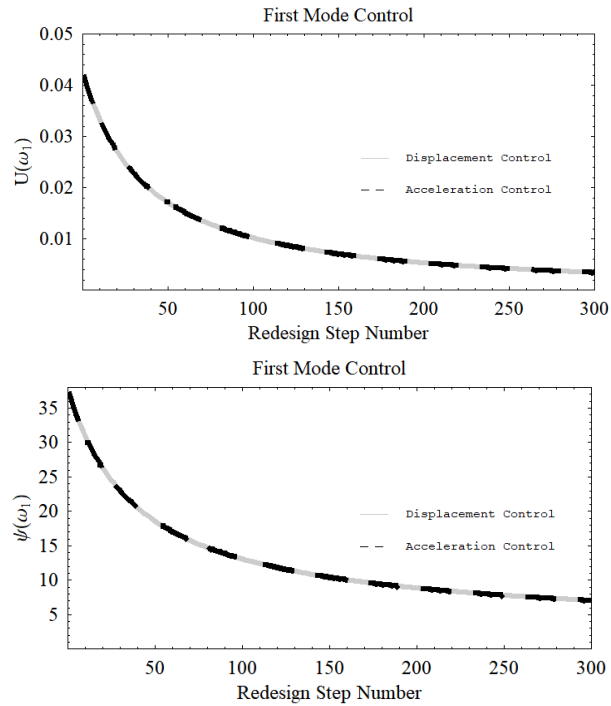
Figure 4. Change of objective function

Figure 4 shows the change in the transfer function amplitude of the end displacement [50] and absolute acceleration at the support, defined as the objective function, during the optimization phase. It is seen that the objective function amplitude, which is a positive value, is reduced in the design steps.

Figure 5. Distribution of optimum stiffness and damping coefficients with displacement control

Figure 6. Distribution of optimum stiffness and damping coefficients with acceleration control

Displacement and acceleration controlled analyses were carried out, taking the first mode into consideration. The optimum stiffness and damping coefficients for the first mode found in the study where the objective function for displacement and absolute acceleration were used, were added to the 6th node as k_6=8.0 10^5 N/m and c_6=6.0 10^3 Ns/m. At the end of the design, the optimum stiffness and damping coefficients found for the first mode were added to the nodes at the end and are drawn in Figures 5 and 6.
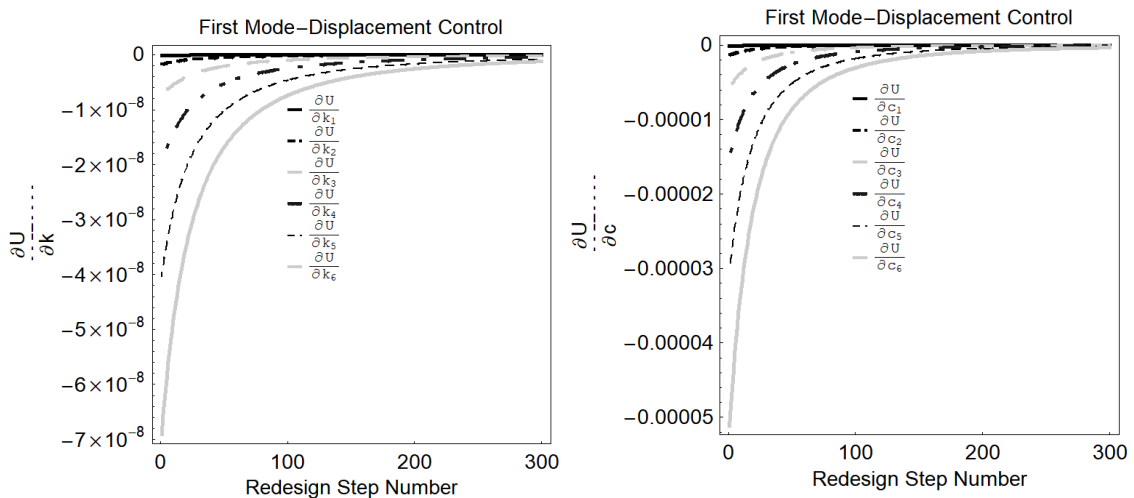
Figure 7. Variation of first order partial derivatives of the objective function for displacement according to stiffness and damping coefficients
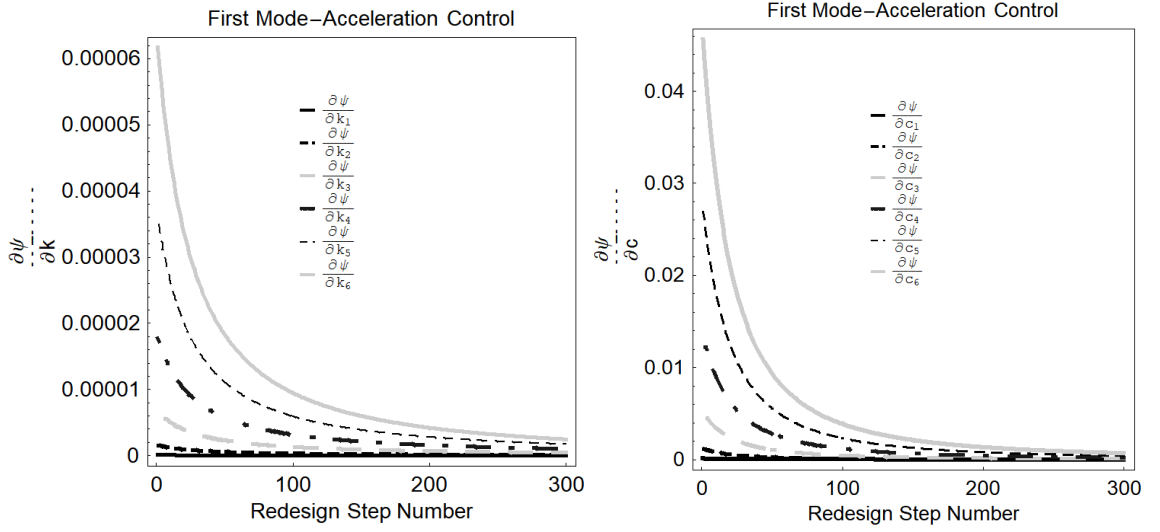
Figure 8. Variation of first order partial derivatives of the objective function for absolute acceleration according to stiffness and damping coefficients

Figures 7 and 8 show the changes of the first-order derivatives of the objective functions for displacement and absolute acceleration according to the design variables (stiffness and damping) in the design steps of the optimization according to the first mode. It can be seen from these graphs that the optimality criteria are met and convergence occurs.

2.3.2 According to the second mode

To apply the optimization algorithm explained in the subject, $\omega = \omega_2$ was first selected, the selected total stiffness amount ($\bar{K} = 1.0 \; 10^7 \; N/m$) and the total damping amount ($\bar{C} = 6.0 \; 10^4 \; Ns/m$) is placed optimally according to the second mode of the structure.
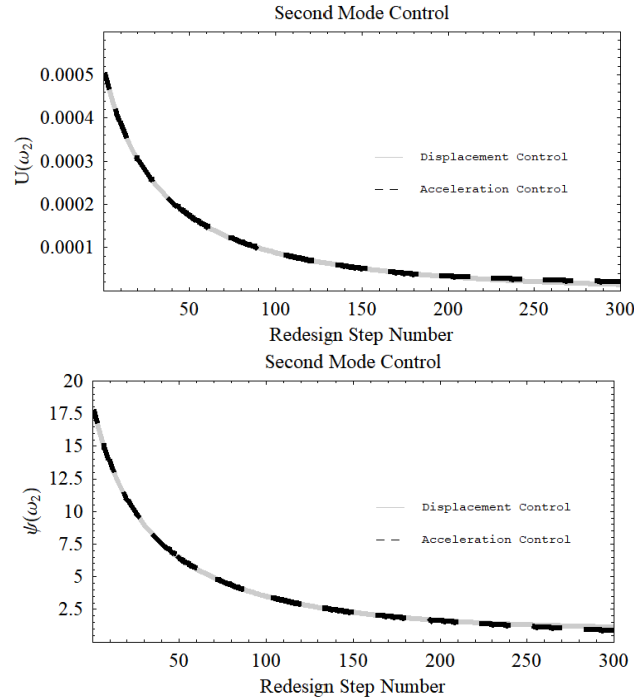
Figure 9. Change of objective function

Figure 9 shows the change in the transfer function amplitude of the tip displacement [50] and absolute

acceleration at the support, defined as the objective function, in the optimization phase. It is seen that the objective function amplitude, which is a positive value, is reduced in the design steps.
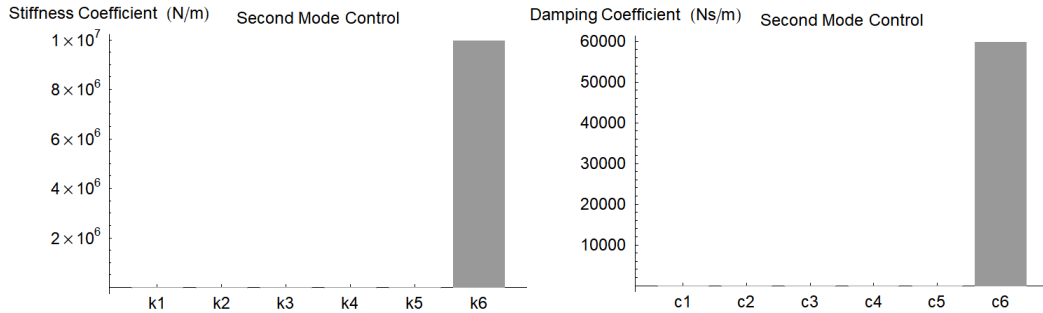
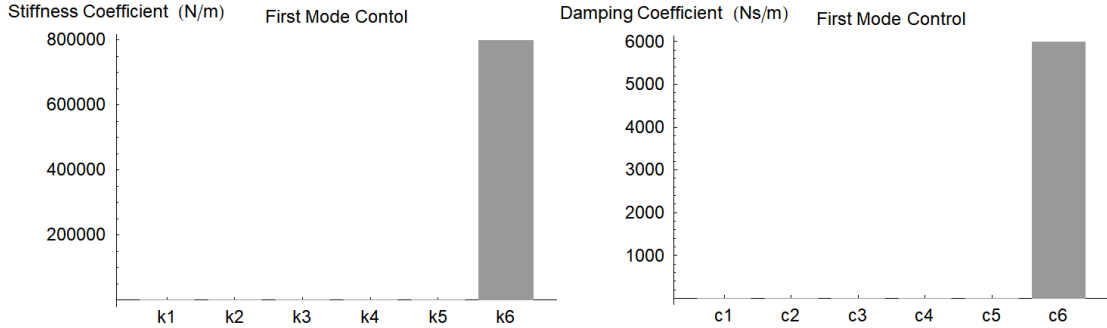**Figure 10.** Distribution of optimum stiffness and damping coefficients with displacement control
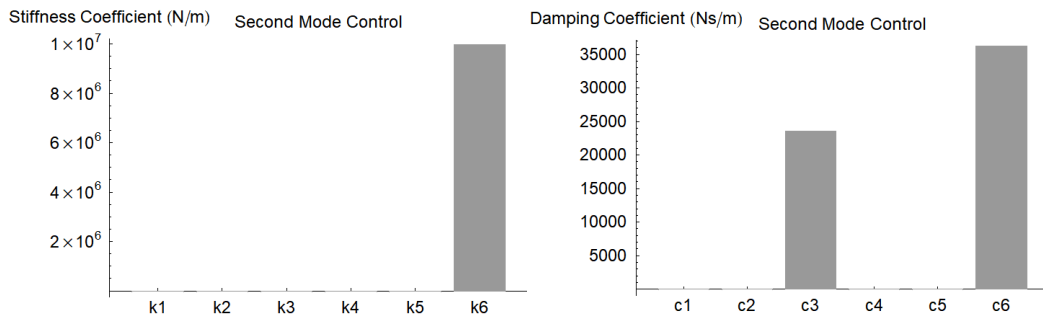
Figure 11. Distribution of optimum stiffness and damping coefficients with acceleration control

Displacement and acceleration controlled analyses were carried out, taking the second mode into account. The optimum stiffness and damping coefficients for the second mode found in the study where the objective function for displacement was used were added to the 6th node as k_6=1.0 10^7 N/m and c_6=6.0 10^4 Ns/m. Here, the optimum stiffness and damping coefficients for the second mode are added to the extreme node. In the study where the objective function for absolute acceleration was used, the optimum stiffness and damping coefficients for the second mode were added as c_3=2.38 10^4 Ns/m to the 3rd node, k_6=1.0 10^7 N/m and c_6=3.62 10^4 Ns/m to the 6th node. The optimum stiffness and damping coefficients found for the second mode at the end of the design are drawn in Figures 10 and 11.
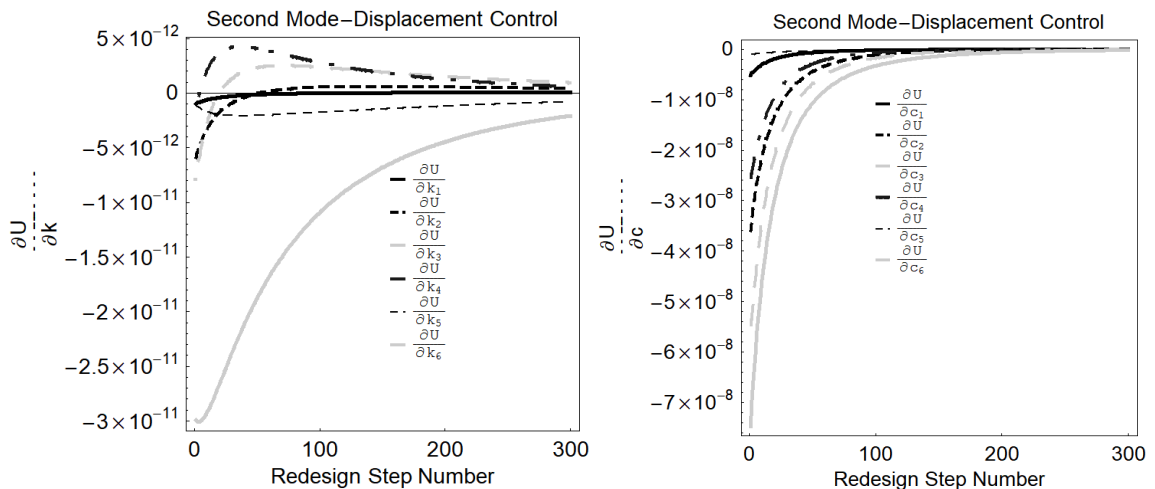
Figure 12. Variation of first order partial derivatives of the objective function for displacement according to stiffness and damping coefficients
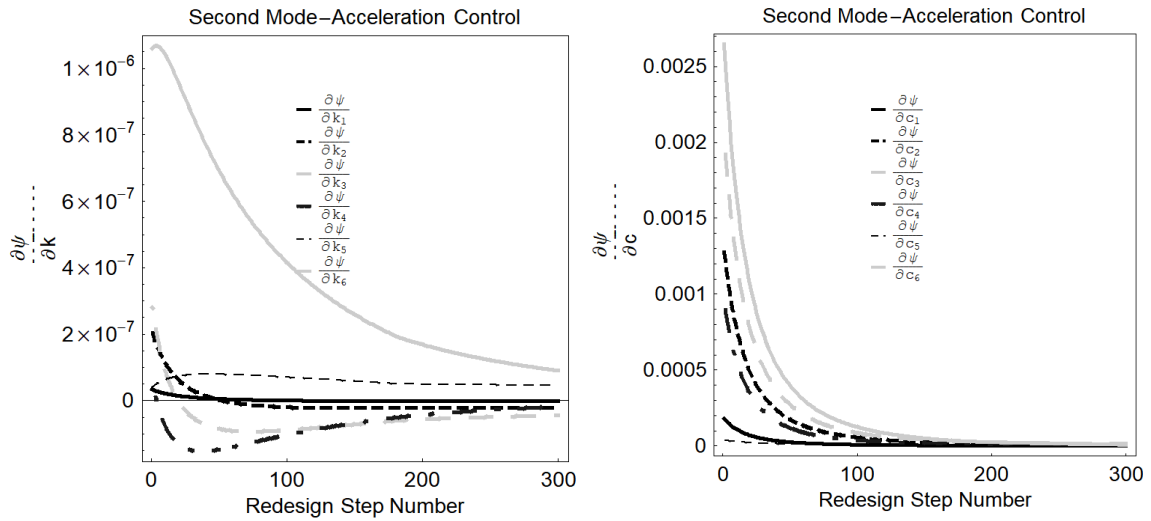
Figure 13. Variation of first order partial derivatives of the objective function for absolute acceleration according to stiffness and damping coefficients

Figures 12 and 13 show the changes of the first-order derivatives of the objective functions for displacement and absolute acceleration according to the design variables (stiffness and damping) in the design steps of the optimization according to the second mode. It can be seen from these graphs that the optimality criteria are met and convergence occurs. In the second mode, it has been observed that convergence based on absolute acceleration is more successful than convergence based on displacement.

2.3.3 According to the third mode

To apply the optimization algorithm explained in the subject, $\omega = \omega_1$ was first selected, the selected total stiffness amount ($\bar{K} = 5.0\,10^7\,N/m$) and the total damping amount ($\bar{C} = 1.2\,10^5\,Ns/m$). is placed optimally according to the third mode of the structure.
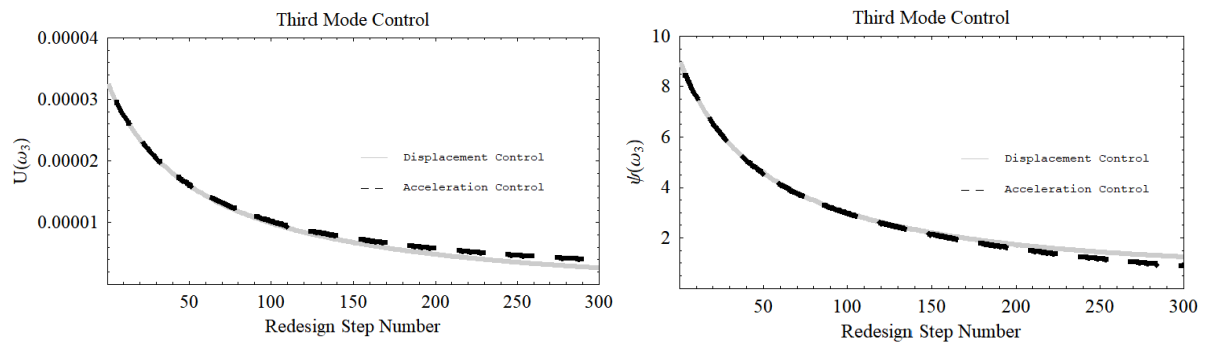
Figure 14. Change of objective function

Figure 14 shows the change in the transfer function amplitude of the tip displacement [50] and absolute acceleration at the support, defined as the objective function, during the optimization phase. It is seen that the objective function amplitude, which is a positive value, is reduced in the design steps.
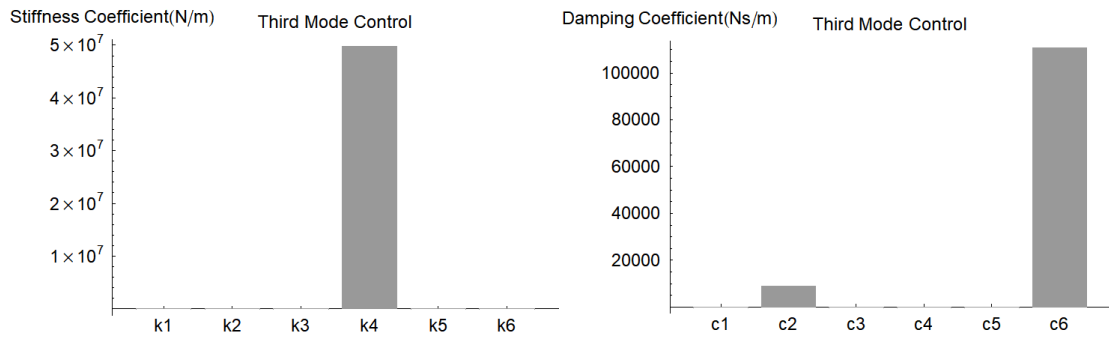
Figure 15. Distribution of optimum stiffness and damping coefficients with displacement control
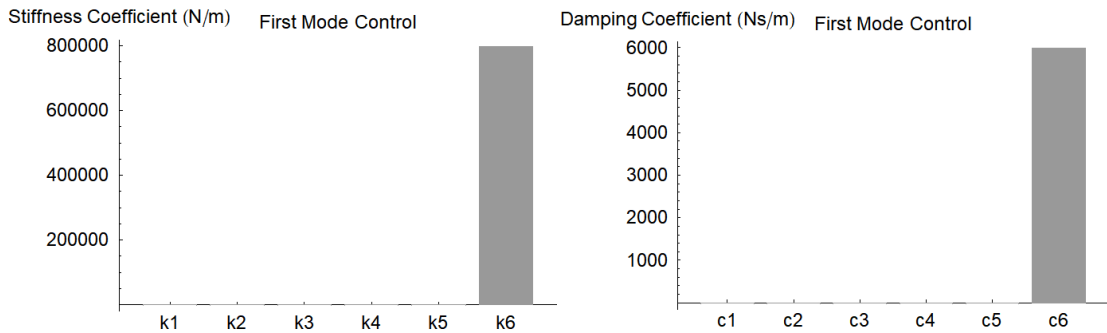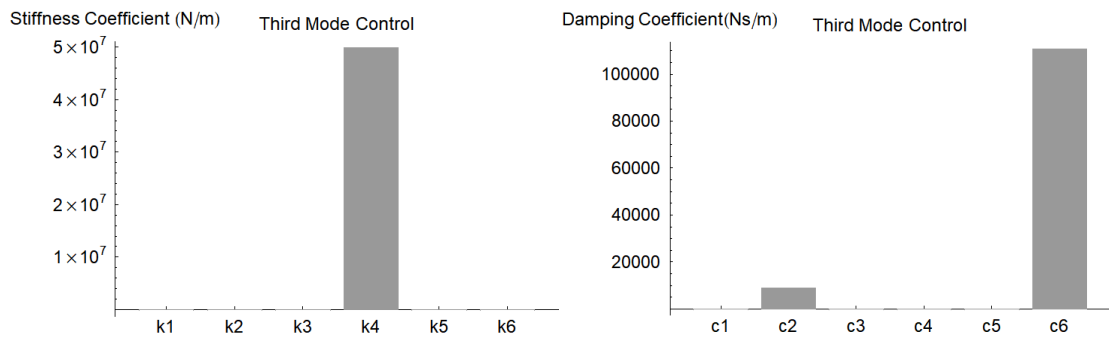

Figure 16. Distribution of optimum stiffness and damping coefficients with acceleration control

Displacement and acceleration controlled analyses were carried out, taking the third mode into account. The optimum stiffness and damping coefficients for the third mode found in the study where the objective function for displacement was used were added as c_2=8.8 10^3 Ns/m to the 2nd node, k_4=5.0 10^7 N/m to the 4th node and c_6=1.11 10^5 Ns/m to the 6th node. In the study where the objective function was used for absolute acceleration, the optimum stiffness and damping coefficients for the third mode were added as c_2=7.32 10^4 Ns/m to the 2nd node, k_6=5.0 10^7 N/m and c_6=4.68 10^4 Ns/m to the 4th node. The optimum stiffness and damping coefficients found for the third mode at the end of the design are drawn in Figures 15 and 16.
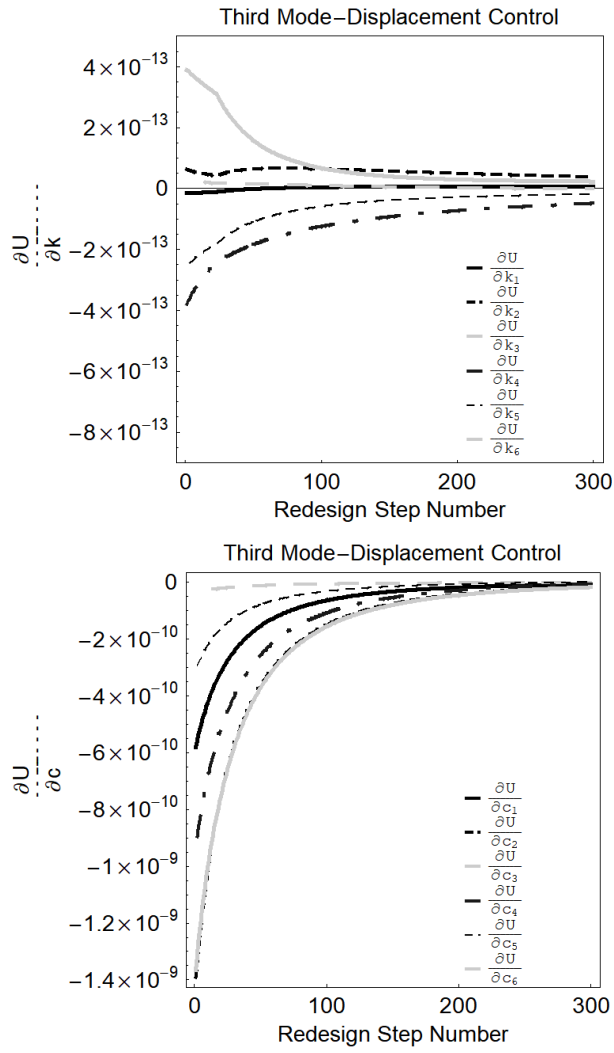
Figure 17. Variation of first order partial derivatives of the objective function for displacement according to stiffness and damping coefficients
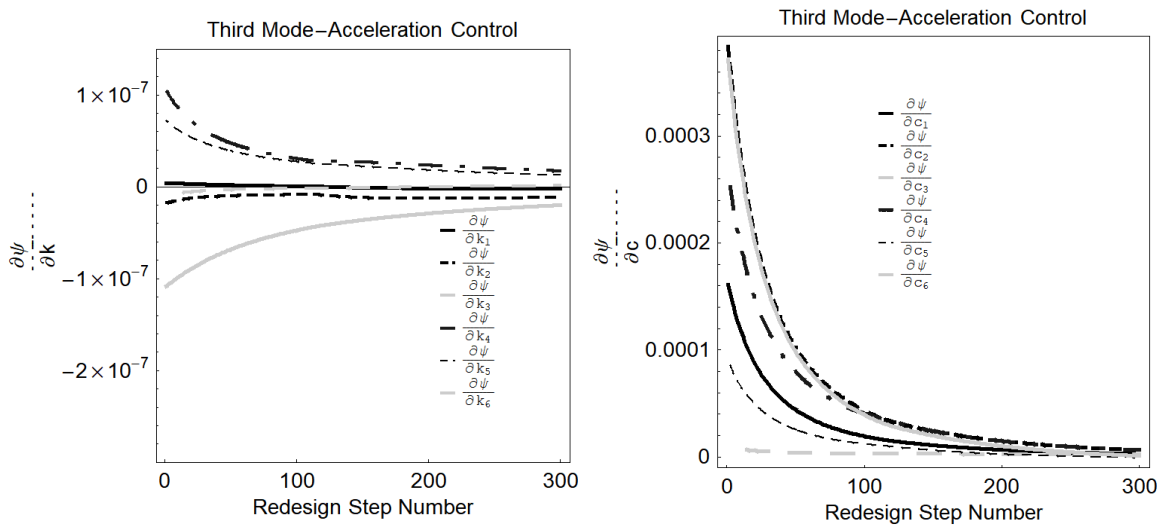

Figure 18. Variation of first order partial derivatives of the objective function for absolute acceleration according to stiffness and damping coefficients

Figures 17 and 18 show the changes in the first-order derivatives of the objective functions for displacement and absolute acceleration according to the design variables (stiffness and damping) in the design steps of the optimization considering the third mode. It can be seen from these figures that the optimality criteria are met and convergence occurs. In the third mode, it has been observed that convergence based on absolute acceleration is more successful than convergence based on displacement.
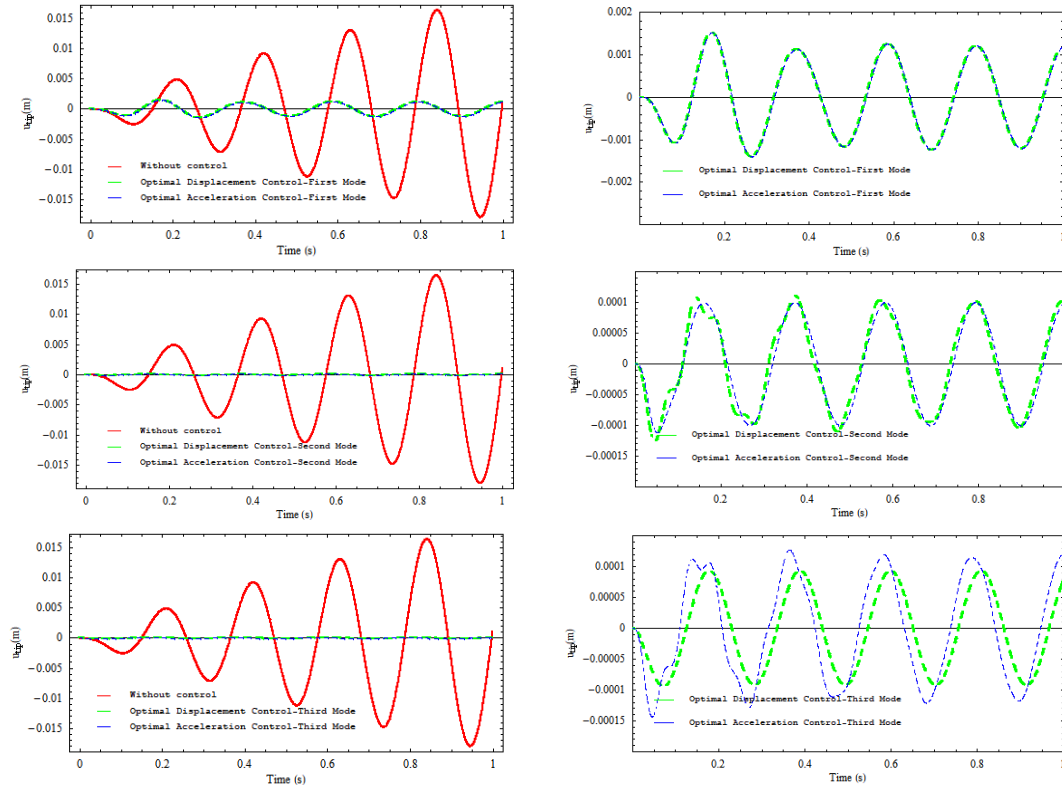
**Figure 19.** The time histories of the tip displacement under the harmonic base acceleration

The optimal design is examined in the frequency domain, and the time response of the tip displacement and absolute acceleration of the optimum designs found are also investigated. The optimum design for the first three modes is compared to the results found in the model without visco-elastic support. The resonance behavior of the beam with both optimal supports and without support is checked by using time history analyses under harmonic loads. Thus, the vertical support acceleration of excitation is chosen as $\ddot{u}_g = Sin(\omega_n t)$ $n = 1,2,\ldots,6$). As a result of the time history analyses, Figures 19 and 20 clearly show that the optimal stiffness and damping designs found with the investigated method can drastically decrease the tip displacement and absolute acceleration. It can be seen that the optimal support designs improve the behaviour of the beam in terms of displacement and acceleration. As can be seen from Figure 20, optimum designs perform better in the first three modes than without viscoelastic support cases. Figures 19 and 20 present the time histories of the tip displacements and the tip absolute accelerations during one second. The graphs (Figures 19 and 20) on the right in both figures are the subtracted versions of the graphs on the left, which have no support. That is, the graphs (Figures 19 and 20) on the right only show the behavior of the optimum designs, not the behavior of the visco-elastic supported case. The first mode response can be dominant in some engineering problems, while another mode can be a priority in other designs. Therefore, in this study, each mode of behavior is considered independently of each other and optimum designs are found accordingly.
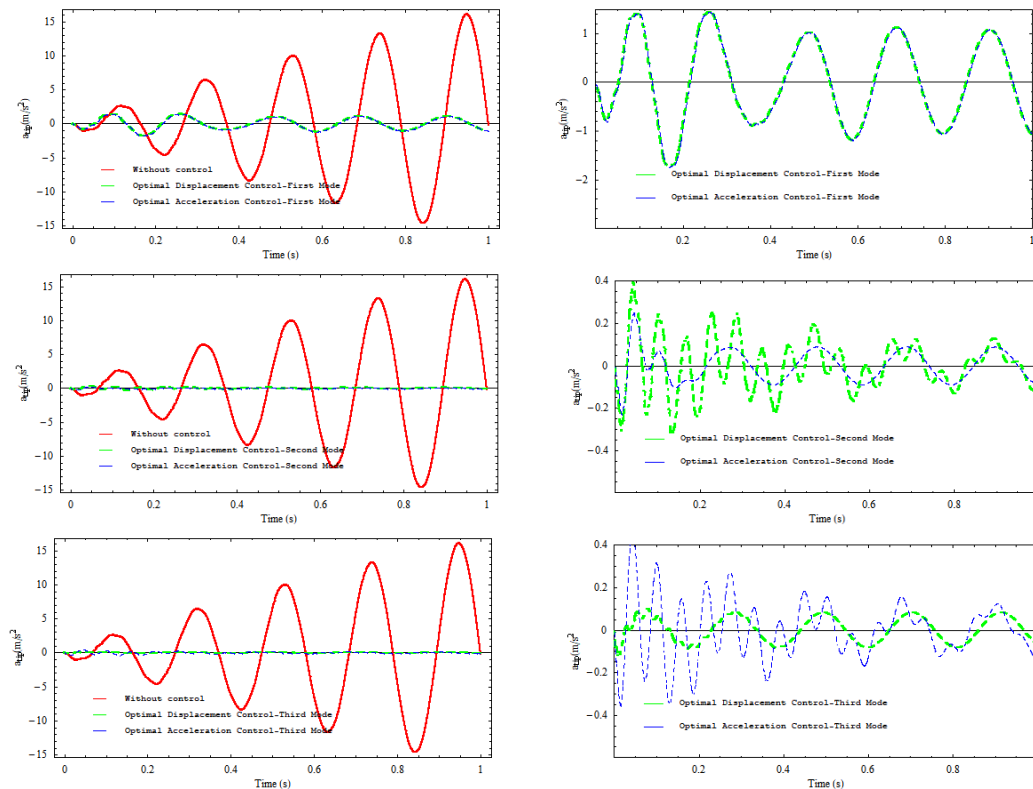
Figure 20. The time histories of the tip acceleration under the harmonic base acceleration

3. CONCLUSIONS

This article illustrates a technique for designing the supports of a Timoshenko cantilever beam supported by viscoelastic elements. As viscoelastic support, a damper and spring are utilized. Consequently, the primary focus of this research is the optimal configuration of the rigidity coefficient and simultaneous damping coefficient. The investigation focused on the determination of the optimal locations and quantities of dampers and springs, which were defined as viscoelastic supports positioned at the nodes, using finite elements to analyze a cantilever Timoshenko beam. In order to achieve this objective, transfer functions were implemented in the optimization problem, optimality criteria were established, and analytical sensitivity formulations were derived for their solution. In the prior displacement-controlled investigation, sole consideration was given to the initial mode. The objective functions were optimized with the absolute acceleration and displacement values for the beam end considered. An optimal viscoelastic support design is one in which the desirable mode behavior can be minimized, as demonstrated by numerical analysis. The optimal configuration for both objective functions, as determined by the first mode, yields the most favorable outcomes with regard to absolute acceleration and tip displacement. An analogous outcome was achieved when the displacement objective function was implemented in the second mode. The stiffness coefficient in the objective function for absolute acceleration is observed at the tip node, whereas the damping coefficient is appended to both the tip and intermediate nodes, as per the second mode. Ultimately, it was noted that the nodes in the third mode, which incorporated the damping and stiffness coefficients, exhibited a marginal distinction from those in the initial two modes. When examining the distribution of spring stiffness coefficients in the third mode control, the identical node is positioned in both objective functions. In displacement control, the damping coefficients are distributed to the second and sixth nodes; in acceleration control, they are distributed to the second and fourth nodes. Time history analyses conducted under harmonic loads reveal that acceleration-based designs exhibit superior acceleration reduction capabilities, while displacement-

based designs demonstrate superior displacement reduction.

Declaration of Ethical Standards

The author declares that all ethical guidelines including authorship, citation, data reporting, and publishing original research are followed.

Declaration of Competing Interest

The author declares that there is no conflict of interest.

Funding / Acknowledgements

This study did not receive funding from any provider.

REFERENCES

[1]   S. I. Timoshenko, D. H. Young and W. Weaver, "Vibration Problems in Engineering", in *John Wiley & Sons*, 1974.

[2]   H. Wei, and Z. Yida, "The dynamic response of a viscoelastic Winkler foundation-supported elastic beam impacted by a low velocity projectile," *Computers & Structures*, vol. 52, no.3, Aug., pp. 431-436, 1994.

[3]   J. H. Chung, W. H. Joo, and K. C. Kim, "Vibration and Dynamic Sensitivity Analysis of a Timoshenko Beam-Column with Elastically Restrained Ends and Intermediate Constraints," *Journal of Sound and Vibration,* vol. 167, no. 2, Oct., pp. 209-215, 1993.

[4]   Y. H. Chen, and J. T. Sheu, "Beam on viscoelastic foundation and layered beam," *Journal of Engineering Mechanics*, vol. 121, no. 2, Feb., pp. 340-344, 1995.

[5]   A. V. Metrikine, and H. A. Dieterman," Instability of vibrations of a mass moving uniformly along an axially compressed beam on a viscoelastic foundation," *Journal of Sound and Vibration,* vol. 201, no. 5, Apr., pp. 567-576, 1997.

[6]   B. K. Lee, J. S. Jeong, G. F. Li, and T. K. Jin, "Free Vibrations of Tapered Piles Embedded Partially in An Elastic Foundation," *Chinese Journal of Geotechnical Engineering,* vol. 21, no. 5, Sep., pp. 609-613, 1999.

[7]   F. Zhen-yu, W. Zhong-min, and F. Li-jian, "Dynamic Stability Analysis of Visco-elastic Pile with Point Visco-elastic Supports," *China Journal of Highway and Transport,* vol. 19, no. 1, Jan., pp. 67-70, 2006.

[8]   Y. H. Chen, and Y. H. Huang, "Dynamic stiffness of infinite Timoshenko beam on viscoelastic foundation in moving co-ordinate," *International Journal for Numerical Methods in Engineering*, vol. 48, no.1, Mar., pp. 1-18, 2000.

[9]   Y. H. Chen, Y. H. Huang, and C. T. Shih, "Response of an infinite Timoshenko beam on a viscoelastic foundation to a harmonic moving load," *Journal of Sound and Vibration,* vol. 241 no. 5, Apr., pp. 809-824, 2001.

[10]   M. Ansari, E. Esmailzadeh, and D. Younesian, "Internal-external resonance of beams on non-linear viscoelastic foundation traversed by moving load," *Nonlinear Dynamics,* vol. 61, no. 1, Jan., pp. 163-182, 2010.

[11]   B. Zhen, J. Xu, and J. Sun, "Analytical solutions for steady state responses of an infinite Euler-Bernoulli beam on a nonlinear viscoelastic foundation subjected to a harmonic moving load," *Journal of Sound and Vibration,* vol. 476, Jun., pp. 1-21, 2020.

[12]   D. Y. Zheng, F. T. K. Au, and Y. K. Cheung, "Vibration of vehicle on compressed rail on viscoelastic foundation," *Journal of Engineering Mechanics*, vol. 126, no. 11, Nov., pp. 1141-1147, 2000.

[13]   A. V. Vostroukhov, and A. V. Metrikine, "Periodically supported beam on a visco-elastic layer as a model for dynamic analysis of a high-speed railway track," *International Journal of Solids and Structures,* vol. 40, no. 21, Oct., pp. 5723-5752, 2003.

[14]   A. V. Metrikine, "Steady state response of an infinite string on a non-linear visco-elastic foundation to moving point loads," *Journal of Sound and Vibration,* vol. 272, no. 3-5, May, pp. 1033-1046, 2004.

[15]   C. E. Majorana, and B. Pomaro, "Dynamic stability of an elastic beam with visco-elastic translational and rotational supports," *Engineering Computations,* vol. 28, no. 2, Mar., pp. 114-129, 2011.

[16]   D. Basu, and N. S. V. Kameswara Rao, "Analytical solutions for Euler–Bernoulli beam on visco-elastic foundation subjected to moving load," *International Journal for Numerical and Analytical Methods in Geomechanics,* vol. 37, no. 8, Jan., pp. 945-960, 2013.

[17]   D. Froio, E. Rizzi, F. M. Simões, and A. Pinto da Costa, "DLSFEM–PML formulation for the steady-state response of a taut string on visco-elastic support under moving load," *Meccanica,* vol. 55, no. 4, Oct., pp. 765-790, 2020.

[18]   Z. Dimitrovová, "Dynamic interaction and instability of two moving proximate masses on a beam on a Pasternak viscoelastic foundation," *Applied Mathematical Modelling,* vol. 100, Dec., pp. 192-217, 2021.

[19]   G. Rozvany, "Optimization of Unspecified Generalized Forces in Structural Design," *Journal of Applied Mechanics*, vol. 41, no. 4, Dec., pp.1143–1145, 1974.

[20]   Z. Mróz, and G. I. N. Rozvany, "Optimal Design of Structures with Variable Support Positions," *Journal of Optimization Theory and Applications*, vol. 15, Jan., pp. 85–101, 1975.

[21]   W. Prager, and G. Rozvany, "Plastic Design of Beams: Optimal Locations of Supports and Steps in Yield Moment," *International Journal of Mechanical Sciences*, vol. 17, no. 10, Oct., pp. 627–631, 1975.

[22]   B. Akesson, and N. Olhoff, "Minimum Stiffness of Optimally Located Supports for Maximum Value of Beam Eigenfrequencies," *Journal of Sound and Vibration*, vol. 120, no. 3, Feb., pp. 457–463, 1988.

[23]   J. W. Hou, and C. H. Chuang, "Design Sensitivity Analysis and Optimization of Vibration Beams with Variable Support Locations," In Proc. Design Automation Conference '16, 1990, Chicago, pp. 281–290.

[24]   B. P. Wang, "Eigenvalue Sensitivity with Respect to Location of Internal Stiffness and Mass Attachment," *American Institute of Aeronautics and Astronautics Journal*, vol. 31, no. 4, May, pp. 791–794, 1993.

[25]   B. P. Wang, and J. L. Chen, "Application of Genetic Algorithm for the Support Location Optimization of Beams," *Computers and Structures*, vol. 58, no. 4, Feb., pp. 797–800, 1996.

[26]   K. M. Won, and Y. S. Park, "Optimal Support Position for a Structure to Maximize Its Fundamental Natural Frequency," *Journal of Sound and Vibration*, vol. 213, no. 5, Jun., pp. 801–812, 1998.

[27]   J. D. Aristizabal-Ochoa, "Static, Stability and Vibration of Non-Prismatic Beams and Columns," *Journal of Sound and Vibration*, vol. 62, no. 3, Apr., pp. 441 455, 1993.

[28]   J. K. Sinha, and M. I. Friswell, "The Location of Spring Supports from Measured Vibration Data," *Journal of Sound and Vibration* vol. 244, no. 1, Jun., pp. 137–153, 2001.

[29]   E. Aydin, "Minimum dynamic response of cantilever beams supported by optimal elastic springs," *Structural Engineering and Mechanics*, vol. 51, no. 3, Aug., pp. 377-402, 2014.

[30]   E. Aydin, M. Dutkiewicz, B. Öztürk, and M. Sonmez, "Optimization of elastic spring supports for cantilever beams," *Structural and Multidisciplinary Optimization*, vol. 62, no. 1, Jan., pp. 55-81, 2020.

[31]   E. Aydın, B. Öztürk, and M. Dutkiewicz, "Determination of optimal elastic springs for cantilever beams supported by elastic foundation," In Proc. International Conference on Engineering Mechanics '24, 2018, pp. 33-36.

[32]   D. Wang, and M. Wen, "Vibration Attenuation of Beam Structure with Intermediate Support under Harmonic Excitation," *Journal of Sound and Vibration*, vol. 532, Aug., pp. 1-19, 2022.

[33]   G. Rozvany, and Z. Mróz, "Column Design: Optimization of Support Conditions and Segmentation," *Journal of Structural Mechanics*, vol. 5, no. 3, Dec., pp. 279–290, 1977.

[34]   N. Olhoff, and J. E. Taylor, "Designing Continuous Columns for Minimum Total Cost of Material and Interior Supports," *Journal of Structural Mechanics*, vol. 6, no. 4, Feb., pp. 367–382, 1978.

[35]   N. Olhoff, and B. Akesson, "Minimum Stiffness of Optimally Located Supports for Maximum Value of Column Buckling Loads," *Structural optimization*, vol. 3, Sep., pp.163–175, 1991

[36]   B. K. Lee, J. K. Lee, T. E. Lee, and S. G Kim, "Free Vibrations of Tapered Beams with General Boundary Conditions," *KSCE Journal of Civil Engineering*, vol. 6, no. 3, Sep., pp. 283-288, 2002.

[37]   T. C. Huang, and C. C. Huang, "Free vibrations of viscoelastic Timoshenko beams," *Journal of Applied Mechanics*, vol. 38, no. 2, Jun., pp. 515-521, 1971.

[38]   Z. S. Liu, H. C. Hu, and D. J. Wang, "New Method for Deriving Eigenvalue Rate with Respect to Support Location," *American Institute of Aeronautics and Astronautics Journal*, vol. 34, no. 4, May, pp. 864–866, 1996.

[39]   I. Takewaki, "Optimal Damper Positioning in Beams for Minimum Dynamic Compliance," *Computer Methods in Applied Mechanics and Engineering*, vol. 156, no. 1-4, Apr., pp. 363-73, 1998.

[40]   L. Sun, "A closed-form solution of beam on viscoelastic subgrade subjected to moving loads," *Computers & Structures*, vol. 80, no. 1, Jan., pp. 1-8, 2002.

[41]   M. H. Kargarnovin, D. Younesian, D. J. Thompson, and C. J. C. Jones, "Response of beams on nonlinear viscoelastic foundations to harmonic moving loads," *Computers & Structures*, vol. 83, no. 23-24, Sep., pp. 1865-1877, 2005.

[42]   F. F. Çalım, "Dynamic analysis of beams on viscoelastic foundation," *European Journal of Mechanics-A/Solids*, vol. 28, no. 3, May-Jun., pp. 469-476, 2009.

[43]   T. Mazilu, "Using the green's function method to analyse the response of an infinite wire on visco-elastic support under moving load," *Acta Technica Corviniensis-Bulletin of Engineering*, vol. 6, no. 2, Apr.-Jun.,pp. 35-38, 2013.

[44]   S. M. Abdelghany, K. M. Ewis, A. A. Mahmoud, and M. M. Nassar, "Dynamic response of non-uniform beam subjected to moving load and resting on non-linear viscoelastic foundation," *Beni-Suef University Journal of Basic and Applied Sciences*, vol. 4, no. 3, Sep., pp. 192-199, 2015.

[45]   Z. Dimitrovová, "Complete semi-analytical solution for a uniformly moving mass on a beam on a two-parameter visco-elastic foundation with non-homogeneous initial conditions," *International Journal of Mechanical Sciences*, vol. 144,Aug., pp. 283-311, 2018.

[46]   S. Roy, G. Chakraborty, and A. DasGupta, "Coupled dynamics of a viscoelastically supported infinite string and a number of discrete mechanical systems moving with uniform speed," *Journal of Sound and Vibration*, vol. 415, Feb., pp. 184-209, 2018.

[47]   Z. Dimitrovová, "New semi-analytical solution for a uniformly moving mass on a beam on a two-parameter visco-elastic foundation," *International Journal of Mechanical Sciences*, vol. 127, Jul., pp. 142-162, 2017.

[48]   Z. Dimitrovová, "Semi-analytical solution for a problem of a uniformly moving oscillator on an infinite beam on a two-parameter visco-elastic foundation," *Journal of Sound and Vibration*, vol. 438, Jan., pp. 257-290, 2019.

[49]   W. Huang, and Y. D. Zou, "The dynamic response of an elastic circular plate on a viscoelastic Winkler foundation impacted by a moving rigid body," *JSME international journal, Ser. 3, Vibration, control engineering, engineering for industry*, vol. 35, no. 2, Jul., pp. 274-278, 1992.

[50]   E. Aydın, B. Adıyaman, and Y. E. Kebeli, "Visko-elastik mesnetler üzerine oturan Timoshenko konsol kirişlerinin minimum titreşimi," In Proc. Uluslararası Türk Dünyası Fen Bilimleri ve Mühendislik Kongresi '04, 2022, pp. 1221-1235.

[51]   G. P. Cimellaro, "Simultaneous stiffness–damping optimization of structures with respect to acceleration, displacement and base shear, *Engineering Structures*, vol. 29, no. 11, Nov., pp. 2853-2870, 2007.

BENDING ANALYSIS OF A PERFORATED MICROBEAM WITH LAPLACE TRANSFORM

[1, *] **Büşra UZUN** [iD] , [2] **Mustafa Özgür YAYLI** [iD]

[1,2]*Bursa Uludag University, Engineering Faculty, Civil Engineering Department, Bursa, TÜRKİYE*
[1] buzun@uludag.edu.tr, [2] ozguryayli@uludag.edu.tr

Highlights

- Laplace transform is applied to bending problem of the microbeam.

- Size dependency is considered with the modified couple stress theory.

- Perforation properties are investigated with size effects for the deflections of the microbeam.

- The results presented with this study can be used by designers to model the perforated micro or macro structural elements.

*Corresponding Author: Büşra UZUN, buzun@uludag.edu.tr

BENDING ANALYSIS OF A PERFORATED MICROBEAM WITH LAPLACE TRANSFORM

[1], * Büşra UZUN ⓘD , [2] Mustafa Özgür YAYLI ⓘD

[1,2]*Bursa Uludag University, Engineering Faculty, Civil Engineering Department, Bursa, TÜRKİYE*
[1] buzun@uludag.edu.tr, [2] ozguryayli@uludag.edu.tr

ABSTRACT: In recent years, the analysis of materials and elements with dimensions at nano/micro levels has gained momentum. While analyzing these small-scale materials and elements, higher-order elasticity theories have started to be used instead of classical elasticity theories (CETs). One of these theories, which includes a small-scale parameter in its constitutive equations, is the modified couple stress theory (MCST). In this study, the bending analysis of a cantilever perforated microbeam is investigated by MCST and Euler-Bernoulli (EB) beam theory. First, the perforation characteristics of the microbeam are described and incorporated into the equation governing the bending problem based on the modified couple stress theory found in the literature. Then, the Laplace transform is applied to the governing equation. The known boundary conditions of the cantilever microbeam are substituted into the equation and the inverse Laplace transform is applied to obtain the deflection equation.

Keywords: Laplace transform, Perforated microbeam, Modified couple stress theory, Bending

1. INTRODUCTION

Materials containing regular holes at equal intervals in a sequential manner are called perforated materials. In nuclear power plants, ships, offshore structures, micro-electro-mechanical systems and nano-electro-mechanical systems, a perforated structure is created due to design requirements [1-3]. One-dimensional bending elements made of perforated materials are also called perforated beams. Due to their wide range of applications, the analysis of perforated beams has recently attracted great interest.

Almitani et al. [2] have investigated the perforation effects on the multilayered beam structure. Luschi and Pieri [4] have presented a study investigating the parameters of perforated beams. Abdelrahman et al. [5] have studied the free and forced dynamics of perforated thick and thin beams. For this purpose, Euler-Bernoulli (EB) and Timoshenko beam theories have been considered and also, the rotary inertia effect has been investigated in the study [5]. Assie et al. [6] have examined the vibration response of a perforated Timoshenko beam affected by a moving load by using the Ritz method. Also in the study, the authors have adopted the Newmark average acceleration method to obtain the time response. Almitani et al. [7] have examined the free and forced vibrations of perforated thin beams by using the semi-analytical mixed Galerkin Laplace method. Eltaher et al. [8] have analyzed the vibrations and stresses of perforated rotated beams via a computational finite element model.

As can be seen from Refs. [5-8], free vibration, forced vibration and stress analyses of perforated beams are presented with various solution techniques. Then, the analysis of perforated beams at nano and micro scales attracted attention. Many authors who presented the analyses at these scales have carried out their studies by taking into account the theories of higher-order elasticity. Bourouina et al. [9] have considered the size effect based on the nonlocal elasticity theory in conjunction with EB and shear deformable beam theories for perforated nanobeams. Kerid and Bounnah [10] have investigated the pull-in voltage of perforated cantilever nanobeam (nanoswitch) via nonlocal elasticity theory. Kafkas et al. [11] have investigated the vibrational frequencies of perforated nanobeams affected by thermal loads based on the nonlocal strain gradient theory. Abdelrahman et al. [1,12] have presented the vibration and bending of perforated beams based on the modified couple stress theory (MCST).

In this study, the MCST will be used as the size-effective theory and the Laplace transform will be used as the solution method. These two main themes are also adopted by the many researchers. Park and Gao [13] have proposed the modified couple stress solution of bending of the Euler-Bernoulli cantilever beam affected by a concentrated point load. Sobhy and Zenkour [14] have studied the static of viscoelastic nano-scaled beams resting on visco-Pasternak foundations via the MCST and different beam theories. Awrejcewicz et al. [15] have studied the thermoelastic vibrations of a nonlinear thick microbeam by using the MCST. Yaylı [16] has proposed the bending analysis of a homogeneous microbeam in conjunction with the Laplace transform and the MCST. Nazmul and Devnath [17] have explored the bending deflection of bi-directional functionally graded nanobeams based on the nonlocal elasticity theory and Laplace transform. Bian and Qing [18] have adopted the Laplace transform method to investigate the stability and dynamic of the nonlocal strain gradient integral model of the Bernoulli-Euler beam. Ike et al. [19] have applied the Laplace transform to solve the buckling problem of moderately thick beams. Li et al. [20] have studied the size-dependent bending response of the Euler–Bernoulli beam based on the Laplace transform.

In this study, the static equation of a perforated microbeam based on the MCST is solved using the Laplace transform. As a continuation of the work presented by Yaylı [16], this study aims to investigate the parameters describing the properties of a perforated microbeam and also to show the effect of size. The bending equation for the perforated microbeam including the filling ratio, the number of holes and the material length scale parameter is obtained. Then, the static displacement curves of a uniformly distributed loaded perforated microbeam are analyzed to show the effect of the filling ratio, number of holes and material length scale parameter.

2. MATERIAL AND METHODS

In this part of the study, for the first step, the calculation of the properties of a microbeam composed of perforated material will be shown. The properties of a microbeam made of perforated material depend on the number of holes and the filling ratio. Then the bending relations based on the MCST will be presented in a form adapted to the perforated microbeam. Finally, the formula for the deflection of a cantilever microbeam will be calculated by applying the Laplace transform.

2.1. Properties of perforated materials

Figure 1 shows a perforated microbeam with length L, width b and height h. To calculate the bending stiffness ($\overline{EI}$) of this perforated microbeam to be investigated, the following equation is presented [4]:

$$\overline{EI} = EI \frac{\beta(N+1)(N^2 + 2N + \beta^2)}{(1 - \beta^2 + \beta^3)N^3 + 3\beta N^2 + \beta^2 N(3 + 2\beta - 3\beta^2 + \beta^3) + \beta^3} \tag{1}$$

In Equation (1), E represents the modulus of elasticity, I specifies the moment of inertia and is caculated by I=bxh³/12, β is the filling ratio and N is the number of holes. Similarly, shear stiffness ($\overline{GA}$) is introduced as follows [4]:

$$\overline{GA} = EA \frac{\beta^3(N+1)}{2N} \tag{2}$$

Here, A is the cross-sectional area of the solid beam and is defined by A=bxh.
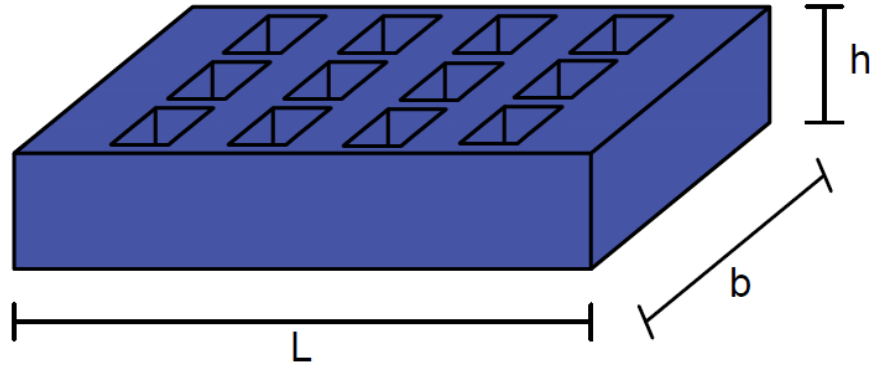
Figure 1. Demonstration of a perforated microbeam

2.2. Bending based on the modified couple stress theory

MCST is a higher-order elasticity theory presented by Yang et al. [21] and introduced to perform size effect-dependent analyses of nano/microelements. This theory defines the strain energy (U) for a linear elastic material as follows [21]:

$$U = \int_V (\boldsymbol{\sigma}:\boldsymbol{\varepsilon} + \boldsymbol{m}:\boldsymbol{\chi})dV \tag{3}$$

here, σ, ε, m and χ are the tensors of stress, strain, deviatoric part of couple stress and symmetric curvature, respectively. By using the defined parameters and displacement fields of Euler-Bernoulli beam, U is re-written as follows [13]:

$$U = -\frac{1}{2}\int_0^L M_y \frac{d^2w(x)}{dx^2}dx - \frac{1}{2}\int_0^L Y_{xy}\frac{d^2w(x)}{dx^2}dx \tag{4}$$

here, $w(x)$ is the transverse deflection, M_y and Y_{xy} are the resultant moment and couple moment, respectively and they are defined by [13]:

$$M_y = \int_A \sigma_{xx}zdA \tag{5}$$

$$Y_{xy} = \int_A m_{xy}dA \tag{6}$$

For a microbeam affected by transverselly uniformly distributed loads, the work done by the external forces is defined as follows:

$$W = \int_0^L q(x)w(x)\,dx \tag{7}$$
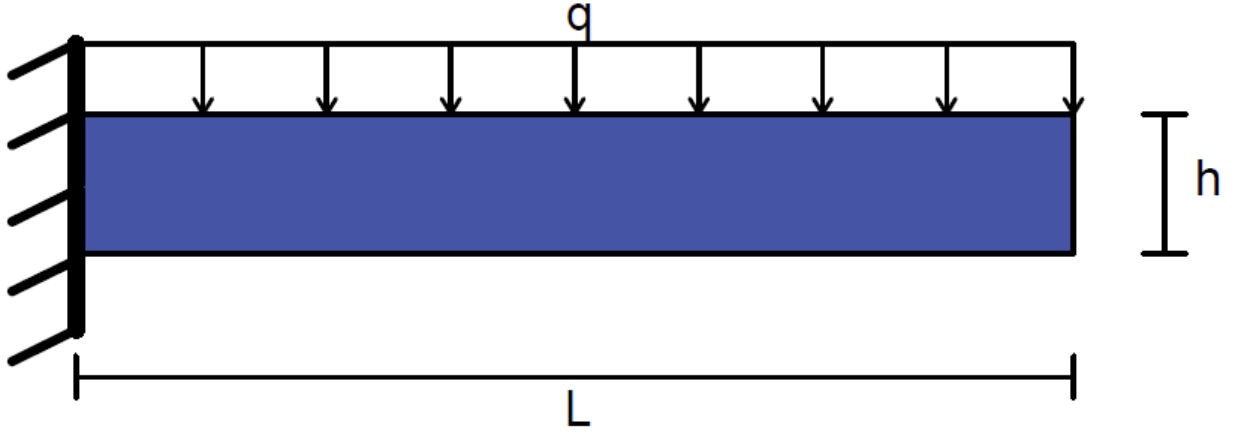
Figure 2. A cantilever perforated microbeam

The total minimum potential energy principle ($\delta\Pi = 0$) can be used to solve this problem and the following equation is established according to this rule:

$$\Pi = U - W = -\frac{1}{2}\int_0^L M_y \frac{d^2w(x)}{dx^2}dx - \frac{1}{2}\int_0^L Y_{xy}\frac{d^2w(x)}{dx^2}dx - \int_0^L q(x)w(x)\,dx \tag{8}$$

With the above equation, the fundamental lemma of calculus of variation is derived as follows [13]:

$$\frac{d^2M_y}{dx^2} + \frac{d^2Y_{xy}}{dx^2} + q(x) = 0 \tag{9}$$

here, M_y and Y_{xy} are defined by:

$$M_y = -\overline{EI}\frac{d^2w(x)}{dx^2} \tag{10}$$

$$Y_{xy} = -\overline{GA}l^2\frac{d^2w(x)}{dx^2} \tag{11}$$

here, l is the material length scale parameter and gives the small-scale effect to the problem. Also, the moment expression (M(x)) based on MCST is obtained as follows:

$$\overline{EI}\frac{d^2w(x)}{dx^2} + \overline{GA}l^2\frac{d^2w(x)}{dx^2} = M(x) \tag{12}$$

If the moment of the beam in Figure 2 is calculated [16]:

$$-\frac{q(x)L^2}{2} - \frac{q(x)x^2}{2} + q(x)Lx = M(x) \tag{13}$$

When this moment expression is substituted in equation (12), the following equation is obtained [16]:

$$\overline{EI}\frac{d^2w(x)}{dx^2} + \overline{GA}l^2\frac{d^2w(x)}{dx^2} = -\frac{q(x)L^2}{2} - \frac{q(x)x^2}{2} + q(x)Lx \tag{14}$$

If the Laplace transform is applied to both sides of equation (14):

$$(\overline{EI} + \overline{GA}l^2)(sw[0] + s^2 w[S] - w'[0]) = -\frac{q(x)L}{s^2} - \frac{q(x)}{s^3} + \frac{q(x)L^2}{2s} \tag{15}$$

is found. From here, $w[S]$ is calculated as follows:

$$w[S] = \frac{-q(x)\big(2 + Ls(-2 + Ls)\big) + 2s^3(sw[0] + w'[0])(\overline{EI} + \overline{GA}l^2)}{2s^5(\overline{EI} + \overline{GA}l^2)} \tag{16}$$

When the boundary conditions $w[0]$ and $w'[0]$ are considered for the clamped end of the beam and the inverse Laplace transform is applied, $w(x)$ is found as follows:

$$w(x) = -\frac{q(x)x^2(x^2 + 6L^2 - 4Lx)}{24(\overline{EI} + \overline{GA}l^2)} \tag{17}$$

3. RESULTS AND DISCUSSION

In this section, using the deflection expression obtained in equation (17), the deflection curves of a perforated microbeam are investigated for various parameters. The material properties of the microbeam are chosen as follows: E=1.44 GPa, ν=0.38 [13]. The microbeam properties are as follows: b=17.6 μm, h=2b μm, L=10h μm. Also, l is considered as 17.6 μm. Finally, the following equation is used to calculate the shear modulus:

$$G = \frac{E}{2(1 + \nu)} \tag{18}$$

First, the effect of the filling ratio β on the deflection value of the cantilever perforated microbeam is analyzed by presenting Figure 3. For this example, four different filling ratios with N=4 are compared. It is seen that lower deflection occurs at higher β values. As the stiffness of the perforated microbeam increases as β increases, the deflection decreases.
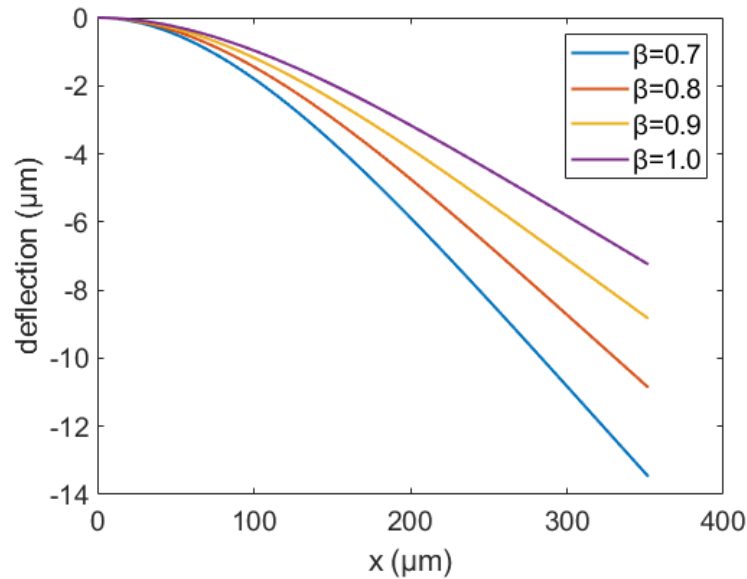
Figure 3. Effect of β on the deflection of a perforated microbeam

In the second example, the effect of the number of holes N on the deflection value of the cantilever perforated microbeam is examined in figure 4. For this example, four different N values with β=0.8 are compared. It is observed that lower deflection occurs at lower N values. Since increasing the number of holes reduces the rigidity of the microbeam, higher deflection values are obtained.
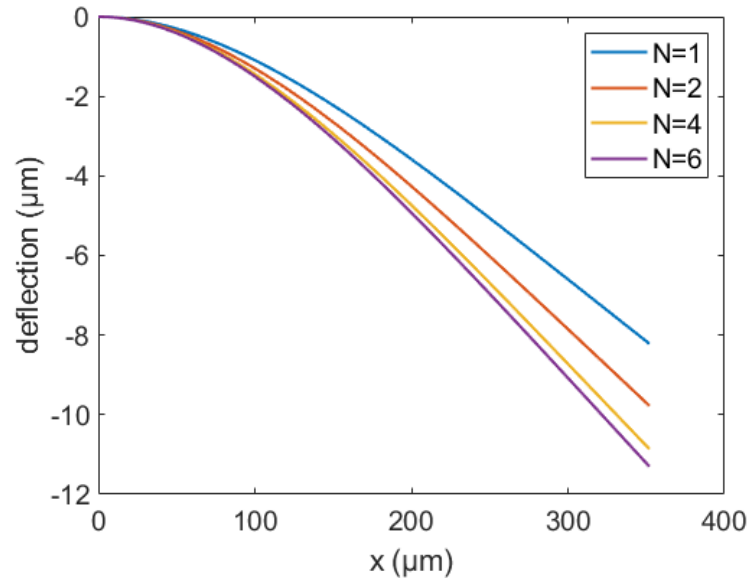
Figure 4. Effect of hole number on the deflection of a perforated microbeam

In the third example, the effect of the MCST on the deflection value of the cantilever perforated microbeam is examined in figure 5. For this example, deflection values based on classical theory and MCST with N=2 and β=0.8 are compared. As can be seen, the deflections obtained with the MCST are smaller than the results of the CET.
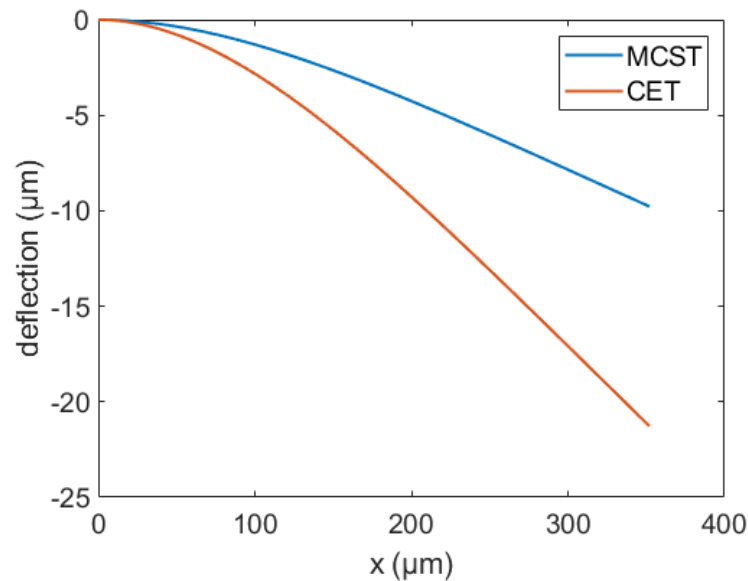
Figure 5. Effect of theory on the deflection of a perforated microbeam

Finally, the effects of l are examined via figure 6. In this example, while the same β and N are used as the previous example, l takes different values from 0 μm to 4b μm. It is understood from the results that as the value of the material length scale parameter increases, the deflection value decreases. It is also worth emphasizing again that at $l = 0$ μm the results reduce to classical elasticity theory.
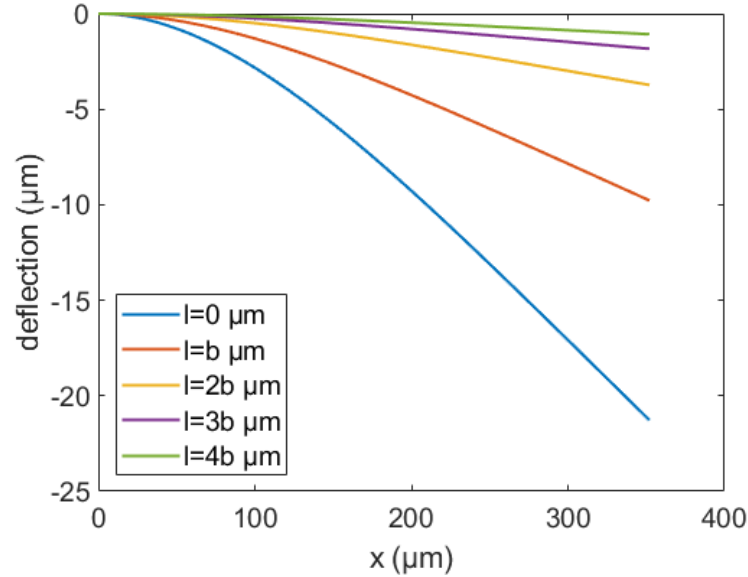
Figure 6. Effect of l on the deflection of a perforated microbeam

4. CONCLUSIONS

In this study, the effect of perforation properties on the deflection of the microbeam is examined with the MCST. The equation governing the bending of the cantilever microbeam under the effect of distributed load and containing the perforation properties is solved by Laplace transform. From the results obtained, it is revealed that the deflection decreased by increasing the filling ratio of the microbeam, and the deflection increased by increasing the number of holes. However, it is revealed that the MCST strengthened the beam and reduced deflection. Taking the material length scale parameter as zero reduces the results to the classical theory, and the deflection values of the microbeam are higher.

Declaration of Ethical Standards

Not applicable.

Credit Authorship Contribution Statement

Büşra UZUN: Conceptualization, Investigation, Methodology, Software, Writing – review, Original draft & editing.
M. Özgür YAYLI: Conceptualization, Investigation, Methodology, Writing - review, Software, Original draft & editing.

Declaration of Competing Interest

Authors declare that there are no declarations of conflict.

Funding / Acknowledgements

Data Availability

This study does not contain usable data.

REFERENCES

[1]   A. A. Abdelrahman, İ. Esen, and M. A. Eltaher, "Vibration response of Timoshenko perforated microbeams under accelerating load and thermal environment," *Applied Mathematics and Computation*, vol. 407, pp. 126307–126307, Oct. 2021, doi: https://doi.org/10.1016/j.amc.2021.126307.

[2]   K. H. Almitani, A. A. Abdelrahman, and M. A. Eltaher, "Influence of the perforation configuration on dynamic behaviors of multilayered beam structure," *Structures*, vol. 28, pp. 1413–1426, Dec. 2020, doi: https://doi.org/10.1016/j.istruc.2020.09.055.

[3]   K. H. Almitani, A. A. Abdelrahman, and M. A. Eltaher, "Stability of perforated nanobeams incorporating surface energy effects," *Steel and Composite Structures*, vol. 35, no. 4, pp. 555–566, Jan. 2020, doi: https://doi.org/10.12989/scs.2020.35.4.555.

[4]   L. Luschi and F. Pieri, "An analytical model for the determination of resonance frequencies of perforated beams," *Journal of Micromechanics and Microengineering*, vol. 24, no. 5, p. 055004, Apr. 2014, doi: https://doi.org/10.1088/0960-1317/24/5/055004.

[5]   A. Abdelrahman, M. A. Eltaher, A.M. Kabeel, A. M. Abdraboh, and A. A. Hendi, "Free and forced analysis of perforated beams," *Steel and Composite Structures*, vol. 31, no. 5, pp. 489–502, Jan. 2019, doi: https://doi.org/10.12989/scs.2019.31.5.489.

[6]   E. Assie, Ş. D. Akbaş, A. H. Bashiri, A. A. Abdelrahman, and M. A. Eltaher, "Vibration response of perforated thick beam under moving load," *The European Physical Journal Plus*, vol. 136, no. 3, Mar. 2021, doi: https://doi.org/10.1140/epjp/s13360-021-01224-2.

[7]   K. H. Almitani, A. A. Abdelrahman, and M. A. Eltaher, "On forced and free vibrations of cutout squared beams," *Steel and Composite Structures*, vol. 32, no. 5, pp. 643–655, Jan. 2019, doi: https://doi.org/10.12989/scs.2019.32.5.643.

[8]   M. A. Eltaher, H. E. Abdelmoteleb, A. A. Daikh, and A. A. Abdelrahman. "Vibrations and stress analysis of rotating perforated beams by using finite elements method", *Steel and Composite Structures*, vol. 41 no. 4, pp. 505, 2021, doi: https://doi.org/10.12989/scs.2021.41.4.505

[9]   H. Bourouina, R. Yahiaoui, R. Kerid, K. Ghoumid, I. Lajoie, F. Picaud and G. Herlem "The influence of hole networks on the adsorption-induced frequency shift of a perforated nanobeam using non-local elasticity theory," *Journal of Physics and Chemistry of Solids*, vol. 136, pp. 109201–109201, Jan. 2020, doi: https://doi.org/10.1016/j.jpcs.2019.109201.

[10]   Kerid, R., and Bounnah, Y. (2021). Effects of structure design on electrostatic pull-in voltage of perforated nanoswitch with intermolecular surface forces. Journal of Ultrafine Grained and Nanostructured Materials, 54(2), 219-227.

[11]   U. Kafkas, B. Uzun, M. Ö. Yaylı, and G. Güçlü, "Thermal vibration of perforated nanobeams with deformable boundary conditions via nonlocal strain gradient theory," *Zeitschrift für Naturforschung*, vol. 78, no. 8, pp. 681–701, Jun. 2023, doi: https://doi.org/10.1515/zna-2023-0088.

[12]   A. A. Abdelrahman, H. E. Abd-El-Mottaleb, and M. A. Eltaher, "On bending analysis of perforated microbeams including the microstructure effects," *Structural Engineering and Mechanics*, vol. 76, no. 6, pp. 765–779, Jan. 2020, doi: https://doi.org/10.12989/sem.2020.76.6.765.

[13]   S. K. Park and X. L. Gao, "Bernoulli–Euler beam model based on a modified couple stress theory", *Journal of Micromechanics and Microengineering*, vol. 16, no. 11, 2006, doi: https://doi.org/10.1088/0960-1317/16/11/015

[14]   M. Sobhy, and A. M. Zenkour, "The modified couple stress model for bending of normal deformable viscoelastic nanobeams resting on visco-Pasternak foundations," *Mechanics of Advanced Materials and Structures*, vol. 27, no. 7, pp. 525–538, Jul. 2018, doi: https://doi.org/10.1080/15376494.2018.1482579.

[15]   J. Awrejcewicz, V.A. Krysko, С. П. Павлов, M. V. Zhigalov, L. A. Kalutsky, and A. V. Krysko, "Thermoelastic vibrations of a Timoshenko microbeam based on the modified couple stress theory," *Nonlinear Dynamics*, vol. 99, no. 2, pp. 919–943, May 2019, doi: https://doi.org/10.1007/s11071-019-04976-w.

[16]   M. Ö. Yaylı, "Mikro Ölçekteki Bir Konsol Kirişin Değiştirilmiş Gerilme Çifti Teorisine Göre Laplace Dönüşümüyle Eğilme Analizi," 20. ULUSAL MEKANİK KONGRESİ, 2017, pp. 626-629.

[17]   M. Nazmul and I. Devnath, "Closed-form expressions for bending and buckling of functionally graded nanobeams by the Laplace transform," *International Journal of Computational Materials Science and Engineering*, vol. 10, no. 02, pp. 2150012–2150012, Jun. 2021, doi: https://doi.org/10.1142/s2047684121500123.

[18]   P. Bian and H. Qing, "Elastic buckling and free vibration of nonlocal strain gradient Euler-Bernoulli beams using Laplace transform," *ZAMM - Journal of Applied Mathematics and Mechanics*, vol. 102, no. 1, Sep. 2021, doi: https://doi.org/10.1002/zamm.202100152.

[19]   C.C. Ike, C. U., Nwoji, B. O., Mama, H. N., Onah and M. E. Onyia, "Laplace transform method for the elastic buckling analysis of moderately thick beams", *International Journal of Engineering Research and Technology*, vol. 12, no. 10, pp. 1626-1638, 2019.

[20]   C. Li, H. Qing, and C. Gao, "Theoretical analysis for static bending of Euler–Bernoulli using different nonlocal gradient models," *Mechanics of Advanced Materials and Structures*, vol. 28, no. 19, pp. 1965–1977, Jan. 2020, doi: https://doi.org/10.1080/15376494.2020.1716121.

[21]   F. Yang, A. C. M. Chong, D. C. C. Lam, and P. Tong, "Couple stress based strain gradient theory for elasticity," *International Journal of Solids and Structures*, vol. 39, no. 10, pp. 2731–2743, May 2002, doi: https://doi.org/10.1016/s0020-7683(02)00152-x.

ANALYSIS OF ELASTIC LATERAL TORSIONAL BUCKLING OF CANTILEVER I SECTIONS BY THE COMPLEMENTARY FUNCTIONS METHOD

[1, *] **Burkay SİVRİ** [iD] , [2] **Ahmad Reshad NOORI** [iD] , [3] **Beytullah TEMEL** [iD]

[1,3] *Cukurova University, Engineering Faculty, Civil Engineering Department, Adana, TÜRKİYE*
[2] *Istanbul Gelisim University, Engineering and Architecture Faculty, Civil Engineering Department, İstanbul, TÜRKİYE*
[1] bsivri@cu.edu.tr, [2] arnoori@gelisim.edu.tr, [3] btemel@cu.edu.tr

Highlights

- Lateral torsional buckling response of cantilever I and IPE beams is performed.
- The effects of loading type on the lateral torsional buckling is examined.
- An effective and accurate numerical method is implemented.

*Corresponding Author: Burkay SİVRİ, bsivri@cu.edu.tr

ANALYSIS OF ELASTIC LATERAL TORSIONAL BUCKLING OF CANTILEVER I SECTIONS BY THE COMPLEMENTARY FUNCTIONS METHOD

1, * Burkay SİVRİ (ID) **, 2 Ahmad Reshad NOORI** (ID) **, 3 Beytullah TEMEL** (ID)

1,3 Cukurova University, Engineering Faculty, Civil Engineering Department, Adana, TÜRKİYE
2 Istanbul Gelisim University, Engineering and Architecture Faculty, Civil Engineering Department, İstanbul, TÜRKİYE
1 bsivri@cu.edu.tr, 2 arnoori@gelisim.edu.tr, 3 btemel@cu.edu.tr

ABSTRACT: In this study, an important stability problem, in the design of cantilever I-beams under lateral torsional buckling behavior is theoretically investigated. The elastic lateral torsional buckling behavior of cantilever I beam loaded from shear centers is examined for four different loading types. The governing differential equation is transformed into a set of first-order ordinary differential equations. The Complementary Functions Method (CFM), which is an effective method in solving the first-order differential equation set, is used. Fifth Order Runge-Kutta (RK5) algorithm is used for numerical integrations in CFM, which can transform the boundary value problem into an initial value problem. The obtained results were compared with the existing results in the literature. It has been shown that CFM can be used effectively in the analysis of elastic lateral torsional buckling behavior of I beams.

Keywords: Complementary functions method, Lateral torsional buckling, Stability

1. INTRODUCTION

The safety of structural elements in terms of lateral torsional buckling is an important issue during the design of structures. In design, safety is evaluated within the framework of limiting the stress values occurring in the structural elements to permissible stresses and the stability of the steady state. To limit the stresses in the sections, the profiles used in steel structures are placed in the structure in a way that the bending moment will be implemented around their strong principal axis. These section profiles, which are considered to be subjected to the bending around their strong principal axes, may twist and buckle around their weak axes at the point with the increased load intensity. In this context, there are many investigations in the literature related to the lateral torsional buckling behavior of beams.

Gupta et al. [1] developed the finite element formulation for the lateral torsional buckling of I beams. They considered the influence of warping deformations and the location of the implemented load in the cross-section in formulations. Sapkás and Kollár [2] examined the stability of thin-walled orthotropic composite beams. They obtained the lateral torsional buckling loads of cantilever beams by considering the influence of shear deformation for several boundary conditions and various types of loadings. Challamel et al. [3] investigated the torsional lateral buckling analysis of cantilever beams with variable cross-section with analytical approaches. They used the finite element approach to verify their results of lateral torsional buckling values obtained for a cantilever beam subjected to a point load to its free end.

The elastic lateral torsional buckling response of cantilever I beams was studied by Özbaşaran [4]. They used the finite difference method in their research. Özbaşaran et al. [5] carried out the critical lateral torsional buckling load of I cantilever beams. They suggested a closed-form solution and verified their results by comparing with those of the ABAQUS. Yilmaz and Kirac [6] studied the lateral torsional buckling response of simply supported IPE and IPN beams. The governing equations were solved for several parameters with the aid of analytical models. They developed an equation that gives the critical lateral torsional buckling loads for various locations of the applied loads in the cross-section of the beam.

Soltani and Asgarian [7] studied the lateral torsional buckling response of axially functionally graded I beams. The stability of beams with various values of material gradient indices was examined. A differential quadrature method was implemented to carry out the lateral torsional buckling loads for hinged–hinged beams subjected to uniformly distributed loads.

In this study, the critical lateral torsional buckling moments of I-section cantilever beams loaded at the shear center with different types of loadings are obtained via the Complementary Functions Method. The lateral torsional buckling behavior of cantilever beams is investigated for different section profiles and beam lengths.

2. GOVERNING EQUATIONS AND PROCEDURE OF THE SOLUTION

A cantilever I beam subjected to a transverse point load to its shear center at the free end is given in Figure 1. The cross-section of the beam is assumed to be symmetric. The governing equation for the lateral torsional buckling of cantilever I beams subjected to a point load at its free end is given by [8] and presented in equation (1).

Figure 1. A cantilever I beam subjected to a point load

$$C_1 \frac{d^4\phi}{dx^4} - C\frac{d^2\phi}{dx^2} - \frac{P^2}{EI_\eta}(L-x)^2 \phi = 0 \tag{1}$$

In this equation; ϕ is the angle of twist, $C_1 = EC_w$ shows the warping rigidity, $C = GI_t$ is the torsional rigidity, P stands for the point load, I_η is the are moment inertia about the weak axis, I_t is tortional moment of inertia, C_w demonstrates the warping constant, E gives the modulus of elasticity and G shows the shear modulus.

By substituting $s = L - x$ in equation (1) it can be simplified in following form:

$$\frac{d^4\phi}{ds^4} - \frac{C}{C_1}\frac{d^2\phi}{ds^2} - \frac{P^2 s^2}{EI_\eta C_1}\phi = 0 \tag{2}$$

The fourth-order ordinary differential equation (2) will be converted to four first-order ordinary differential equations. For this purpose, the new variables can be determined as in equations (3-5).

$$\phi = t_1 \tag{3}$$

$$\frac{d\phi}{ds} = t_2 \tag{4}$$

$$\frac{d^2\phi}{ds^2} = t_3 \tag{5}$$

$$\frac{d^3\phi}{ds^3} = t_4 \tag{6}$$

By using equation 2 and equations (3-6) the set of governing equations of lateral torsional buckling can be obtained as follows:

$$\frac{dt_1}{ds} = t_2 \tag{7}$$

$$\frac{dt_2}{ds} = t_3 \tag{8}$$

$$\frac{dt_3}{ds} = t_4 \tag{9}$$

$$\frac{dt_4}{ds} = \frac{C}{C_1} t_3 + \frac{P^2 s^2}{EI_\eta C_1} t_1 \tag{10}$$

A cantilever I beam subjected to a transverse uniformly distributed load to its shear center is illustrated in Figure 2. The governing equation for the lateral torsional buckling of cantilever I beams subjected to uniformly distributed load is given by [9] and presented in equation (11).
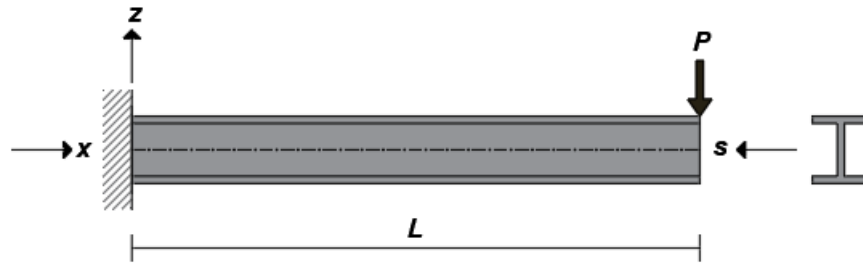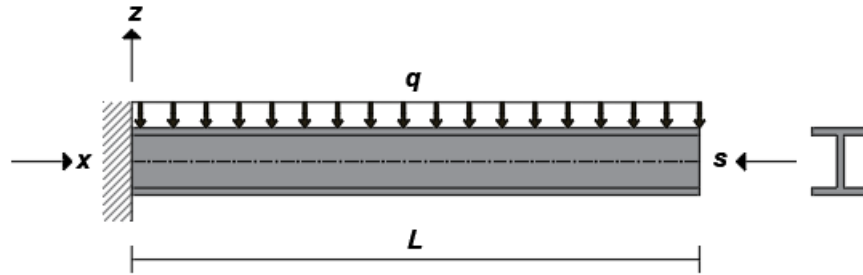

Figure 2. A cantilever I beam subjected to uniformly distributed transverse load

$$\frac{d^4\phi}{ds^4} - \frac{C}{C_1} \frac{d^2\phi}{ds^2} - \frac{q^2 s^4}{4EI_\eta C_1} \phi = 0 \tag{11}$$

In this equation q stands for the magnitude of uniformly distributed load. The variables given in equations (3-6) will be used to convert equation (11) to a set of ordinary canonical differential equations.

$$\frac{dt_1}{ds} = t_2 \tag{12}$$

$$\frac{dt_2}{ds} = t_3 \tag{13}$$

$$\frac{dt_3}{ds} = t_4 \tag{14}$$

$$\frac{dt_4}{ds} = \frac{C}{C_1} t_3 + \frac{q^2 s^4}{4EI_\eta C_1} t_1 \tag{15}$$

A cantilever I beam subjected to a transverse uniformly distributed load and a point load at its free end is presented in Figure 3. The governing equation for the lateral torsional buckling of this cantilever beam is given in [9] and presented in equation (16). The magnitude of the point is taken as $P = \lambda qL$.
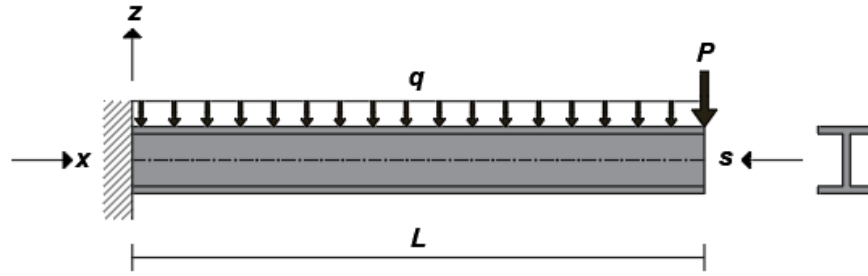
Figure 3. An I cantilever beam subjected to a point load and uniformly distributed load

$$\frac{d^4\phi}{ds^4} - \frac{C}{C_1}\frac{d^2\phi}{ds^2} - \frac{q^2 s^2 (2\lambda L + s)^2}{4EI_\eta C_1}\phi = 0 \tag{16}$$

The variables given previously in equations (3-6) will be used to change equation (16) to a set of canonical differential equations. The obtained equations are written as follows:

$$\frac{dt_1}{ds} = t_2 \tag{17}$$

$$\frac{dt_2}{ds} = t_3 \tag{18}$$

$$\frac{dt_3}{ds} = t_4 \tag{19}$$

$$\frac{dt_4}{ds} = \frac{C}{C_1}t_3 + \frac{q^2 s^2 (2\lambda L + s)^2}{4EI_\eta C_1}t_1 \tag{20}$$

A cantilever I beam subjected to a concentrated moment is shown in Figure 4. The governing equation of the torsional lateral buckling response of this beam is presented by [9] and given in equation (21).
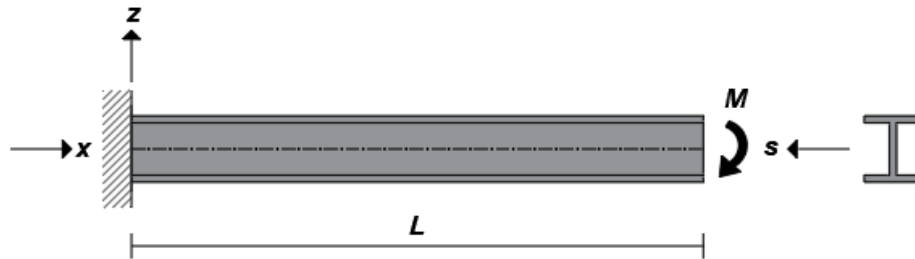
Figure 4. A cantilever I beam subjected to a point moment

$$\frac{d^4\phi}{ds^4} - \frac{C}{C_1}\frac{d^2\phi}{ds^2} - \frac{M^2}{EI_\eta C_1}\phi = 0 \tag{21}$$

By using the variables given in equations (3-6), equation (11) is converted to a set of ordinary canonical differential equations and presented below (equations (22-25).

$$\frac{dt_1}{ds} = t_2 \tag{22}$$

$$\frac{dt_2}{ds} = t_3 \tag{23}$$

$$\frac{dt_3}{ds} = t_4 \tag{24}$$

$$\frac{dt_4}{ds} = \frac{C}{C_1} t_3 + \frac{M^2}{EI_\eta C_1} t_1 \tag{25}$$

The set of canonical equations obtained from equations (2), equations (11), equations (16) and equations (21) are two-point boundary value problems. The CFM will be implemented to carry out the solution of these equations. The main principle is the implemented method is that it reduces a two-point boundary value problem to an initial value problem. The solution of the set of the ordinary differential equations can be given in equation (26) which is consist of four homogenous and one nonhomogeneous solution [10,11]. In the solution procedure of the initial value problem the Runge – Kutta (5th order) will be used [12]. The CFM is an efficient, accurate and easily applicable method for the numerical solution of the two-point boundary value problems. This method was applied successfully to the solution of various structural mechanics problems [13,14].

$$\phi(s) = \phi_0(s) + a_1\phi_1(s) + a_2\phi_2(s) + a_3\phi_3(s) + a_4\phi_4(s) \tag{26}$$

In this equations, $\phi_0(s)$ is the nonhomogeneous solution, $\phi_1(s), \phi_2(s), \phi_3(s), \phi_4(s)$ are homogenous solutions and a_1, a_2, a_3, a_4 are the integrations constants which can be found with the aid of the boundary conditions. The boundary conditions that are required for the solution of the governing equation of the torsional lateral buckling response of the cantilever I beams are listed in Table 1.

Table 1. Boundary conditions

Free end	$C\dfrac{d\phi}{ds} - C_1\dfrac{d^3\phi}{ds^3} = 0$
	$\dfrac{d^2\phi}{ds^2} = 0$
Fixed end	$\dfrac{d\phi}{ds} = 0$
	$\phi = 0$

The governing equation of the torsional lateral buckling of the considered beams is homogenous. Thus, once the integration constants matrix from the homogenous solution of the differential equation is obtained then its determinant can be calculated easily. The set of integrations which makes this determinant zero are the critical lateral torsional buckling loads (P, q or M). These values can be obtained with the method of Secant with the desired accuracy.

3. NUMERICAL EXAMPLES

To validate the accuracy and applicability of the CFM, lateral torsional buckling results of the present paper are compared with those of the available literature. The material and geometric properties of the cantilever I beam are presented in Table 2.

Table 2. Geometric and material properties of the I beam

$E(MPa)$	200000
$G(MPa)$	76923
$I_\eta (x10^4 \ mm^4)$	68.16
$I_t (x10^3 \ mm^4)$	28.20
$C_w (x10^6 \ mm^6)$	3958.9

The lateral torsional buckling moments for this cantilever I beam are calculated and compared with those of Özbaşaran [4] in Table 3. To solve the governing equation with the CFM, $N = \{5, 10, 25\}$ collocations points are used.

Table 3. Comparison of the lateral torsional buckling moments for I sections (kN.m)

$L(m)$		P	q	$P+q(\lambda=1)$	M
	$N=5$	98.93	198.25	120.26	28.34
	$N=10$	98.92	198.20	120.25	28.34
1.5	$N=25$	98.92	198.20	120.25	28.34
	Özbaşaran [4]	98.93	198.19	120.18	28.34
	$N=5$	63.97	124.77	77.33	19.20
	$N=10$	63.97	124.73	77.32	19.20
2	$N=25$	63.97	124.73	77.32	19.20
	Özbaşaran [4]	63.96	124.72	77.28	19.25
	$N=5$	35.63	66.87	42.71	11.44
	$N=10$	35.62	66.84	42.70	11.44
3	$N=25$	35.62	66.84	42.70	11.44
	Özbaşaran[4]	35.61	66.83	42.66	11.47
	$N=5$	24.09	44.06	28.72	8.07
	$N=10$	24.08	44.02	28.71	8.07
4	$N=25$	24.08	44.02	28.71	8.07
	Özbaşaran [4]	24.08	44.00	28.80	8.08

When Table 3 is analyzed, it can be obviously seen that the lateral torsional buckling moments obtained via the CFM are in really good agreement with the existing results presented previously by Özbaşaran [4]. It has been perceived that the results listed in Table 3 ensure sufficient sensibility for the used collocation point when two digits after the decimal are taken into account.

In the subsequent numerical applications, the lateral torsional buckling response of cantilever beams with IPE section will be investigated for four different loading types. The cross-sectional properties of the used IPE profiles are given in Table 4.

Table 4. Goemetric properties of IPE sections

Geometric properties	IPE 120	IPE 180	IPE 220	IPE 270	IPE 330
$I_\eta (x10^4 \ mm^4)$	27.67	100.90	204.90	419.90	788.10
$I_t (x10^3 \ mm^4)$	16.89	47.23	89.82	157.10	275.90
$C_w (x10^6 \ mm^6)$	872	7322	22310	69469	196090

The lateral torsional buckling loads obtained for cantilever IPE beams are listed in Table 5. In the solution of the present problem of different lengths with the CFM, only 10 collocation points are used.

Table 5. Lateral torsional buckling moments obtained for cantilever IPE beams (kNm)

$L(m)$	Profil Tipi	P	q	$P + q(\lambda = 1)$	M
1.5	IPE 120	38.10	72.79	45.85	11.86
	IPE 180	160.06	322.15	194.76	45.51
	IPE 220	360.68	740.53	440.64	99.36
	IPE 270	823.14	1723.99	1009.54	220.20
	IPE 330	1774.78	3762.56	2181.74	466.88
2	IPE 120	25.41	47.25	30.40	8.28
	IPE 180	103.21	202.21	124.88	30.72
	IPE 220	229.28	459.29	278.71	65.70
	IPE 270	512.36	1052.00	625.94	141.13
	IPE 330	1082.96	2261.21	1327.42	290.98
3	IPE 120	14.87	26.68	17.65	5.12
	IPE 180	57.23	107.86	68.67	18.23
	IPE 220	124.64	240.24	150.28	38.18
	IPE 270	271.92	538.80	329.79	79.37
	IPE 330	561.70	1137.35	684.30	158.15
4	IPE 120	10.41	18.26	12.29	3.69
	IPE 180	38.55	70.77	45.99	12.83
	IPE 220	82.60	154.93	99.00	26.53
	IPE 270	177.03	341.26	213.46	54.23
	IPE 330	360.77	711.44	437.11	106.18
5	IPE 120	7.99	13.79	9.40	2.89
	IPE 180	28.79	51.83	34.20	9.86
	IPE 220	60.86	111.86	72.63	20.22
	IPE 270	128.44	242.40	154.16	40.84
	IPE 330	258.82	499.60	312.16	79.09
6	IPE 120	6.47	11.05	7.60	2.37
	IPE 180	22.88	40.59	27.10	8.01
	IPE 220	47.87	86.59	56.93	16.30
	IPE 270	99.69	184.99	119.22	32.61
	IPE 330	198.85	377.22	238.93	62.66

For a better interruption of the parametric studies results of the presented approach, graphical forms of the lateral torsional moments are illustrated in Figures (5-6).

From Table 5 and Figures (5-6) it can be understood that the loading type, section properties, and beam length have a significant effect on the lateral torsional buckling behavior of the problems in the hand. By increasing the length of the beam, the lateral torsional buckling moment of the structures decreases. Among the compared loading cases the concentrated bending moment at free end of the cantilever beam is the most critical case. Among the compared sections IPE120 is the weakest section for lateral torsional buckling of cantilever beams.
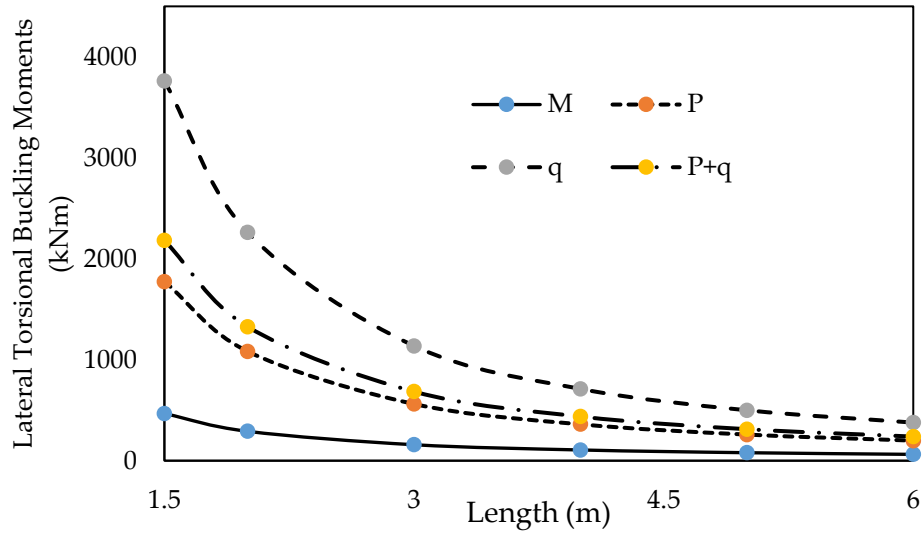
Figure 5. Lateral torsional buckling loads of IPE330 for several types of load
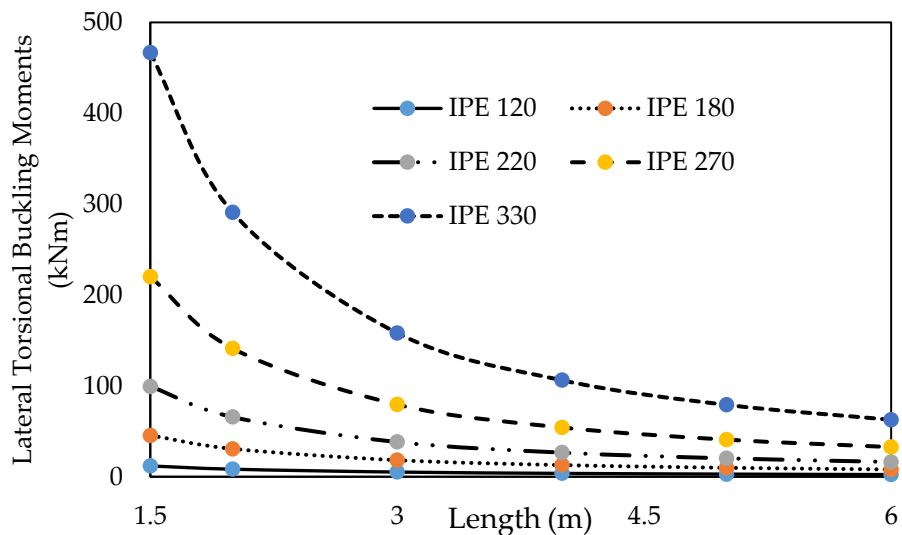
Figure 6. Lateral torsional buckling loads of for various cantilever IPE beams subjected to a point moment

4. CONCLUSIONS

The differential equations governing the lateral torsional buckling behavior of I and IPE section cantilever beams, loaded at their shear center are solved numerically with the CFM for different loading types. Results are obtained for various values of collocation points and the compared with those of the available literature and excellent agreement is observed. This validation demonstrated the applicability and accuracy of the suggested method for lateral torsional buckling analysis of the problem in the hand. The critical lateral torsional moments are carried out for four different types of loading. It has been observed that type of the loading, length of the beam and type of the cross-section of the cantilever beams have important influences on the critical lateral torsional buckling loads. By increasing the length of the length of beam the critical lateral torsional buckling moment decreases. The IPE330 profile has the highest value capacity among the compared cases. The concentrated moment is the most critical loading among

the compared loading cases while the uniformly distributed loading case is the safest case.

Declaration of Ethical Standards

The authors of this article declare that the materials and methods used in this study do not require ethical committee permission and/or legal-special permission.

Credit Authorship Contribution Statement

All the authors contribute in all stages and all sections of the paper.

Declaration of Competing Interest

The authors declare that they have no known competing financial interests or personal relationships that could have appeared to influence the work reported in this paper.

Funding / Acknowledgements

Data Availability

The data that support the findings of this study are available from the corresponding author upon reasonable request.

REFERENCES

[1]   P. Gupta, S. T. Wang, and G. E. Blandford, "Lateral-torsional buckling of nonprismatic I-beams," *Journal of Structural Engineering*, vol. 122, no. 7, pp. 748-755, 1996.

[2]   Á. Sapkás and L. P. Kollár, "Lateral-torsional buckling of composite beams," *International Journal of Solids and Structures*, vol. 39, no. 11, pp. 2939-2963, 2002.

[3]   N. Challamel, A. Andrade, and D. Camotim, "An analytical study on the lateral-torsional buckling of linearly tapered cantilever strip beams," *International Journal of Structural Stability and Dynamics*, vol. 7, no. 03, pp. 441-456, 2007.

[4]   H. Özbaşaran, "Finite differences approach for calculating elastic lateral torsional buckling moment of cantilever I sections," *Anadolu University Journal of Science and Technology A-Applied Sciences and Engineering*, vol. 14, no. 2, pp. 143-152, 2013.

[5]   H. Ozbasaran, R. Aydin, and M. Dogan, "An alternative design procedure for lateral–torsional buckling of cantilever I-beams," *Thin-Walled Structures*, vol. 90, pp. 235-242, 2015.

[6]   T. Yilmaz and N. Kirac, "Analytical and parametric investigations on lateral torsional buckling of European IPE and IPN beams," *International Journal of Steel Structures*, vol. 17, pp. 695-709, 2017.

[7]   M. Soltani and B. Asgarian, "Lateral-torsional stability analysis of a simply supported axially functionally graded beam with a tapered I-section," *Mechanics of Composite Materials*, vol. 56, pp. 39-54, 2020.

[8]   S. P. Timoshenko and J. M. Gere, *Theory of Elastic Stability*, New York: McGraw-Hill, 1961.

[9]   H. Özbaşaran, "Analytical and experimental research of lateral torsional buckling of cantilever steel I-beams (in Turkish)," Ph.D. dissertation, Eskisehir Osmangazi University, Eskisehir, 2013.

[10]   B. Sivri and B. Temel, "Buckling analysis of axially functionally graded columns based on Euler-Bernoulli and Timoshenko beam theories (in Turkish)," *Cukurova University Journal of the Faculty of Engineering*, vol. 37, no. 2, pp. 319-328, 2022.

[11]   A.R. Noori, T.A. Aslan, and B. Temel, "Static analysis of FG beams via complemantary functions method," *European Mechanical Science*, vol. 4, no. 1, pp. 1-6, 2020.

[12]   S.C. Chapra and R. P. Canale, *Yazılım Ve Programlama Uygulamalarıyla Mühendisler İçin Sayısal Yöntemler*, İstanbul: Literatür Yayınevi, 2003.

[13]   Y. Sefa, "Hydrogen elasticity solution of functionally-graded spheres, cylinders and disks." *International Journal of Hydrogen Energy* , vol. 45, no. 41, pp. 22094-22101, 2020.

[14]   K. Celebi, D. Yarimpabuc, and N. Tutuncu, "Free vibration analysis of functionally graded beams using complementary functions method". *Archive of Applied Mechanics*, vol. 88, pp. 729-739, 2018.

COMPARISON OF NUMERICAL ANALYSIS OF A SINGLE-SPAN STEEL PROTOTYPE STRUCTURE AND A SCALE MODEL STRUCTURE UNDER THE EFFECT OF SEISMIC LOADS

[1, *] **Yunus Emre KEBELİ** , [2] **Şeyma TEBERİK** ,[3] **Ersin AYDIN** , [4] **Fatih ÇELİK**

[1,2,3,4]*Niğde Ömer Halisdemir University, Engineering Faculty, Civil Engineering Department, Niğde, TÜRKİYE*
[1] yunusemrekebeli@ohu.edu.tr, [2] teberiksym@gmail.com, [3] eaydin@ohu.edu.tr, [4] fatihcelik@ohu.edu.tr

Highlights

- In this study, a scaling factor (λ=10), which is widely accepted in the literature, was used to design a scaled model to represent a three-storey single-span life-size structure.

- In the analysis of the prototype and scaled structure with the Sap2000 program, time history analyzes were made using the real and scaled earthquake records of El Centro (1940), Kobe (1995) and Northridge (1994).

- The time history analyses of the prototype and the scaled structure were compared by looking at the acceleration and displacement values of each floor and it was seen that the results were close to each other when scaled according to the scaling factor (λ).

*Corresponding Author: Yunus Emre KEBELİ, yunusemrekebeli@ohu.edu.tr

COMPARISON OF NUMERICAL ANALYSIS OF A SINGLE-SPAN STEEL PROTOTYPE STRUCTURE AND A SCALE MODEL STRUCTURE UNDER THE EFFECT OF SEISMIC LOADS

[1, *] **Yunus Emre KEBELİ** [ID], [2] **Şeyma TEBERİK** [ID], [3] **Ersin AYDIN** [ID], [4] **Fatih ÇELİK** [ID]

[1,2,3,4]*Niğde Ömer Halisdemir University, Engineering Faculty, Civil Engineering Department, Niğde, TÜRKİYE*
[1] yunusemrekebeli@ohu.edu.tr, [2] teberiksym@gmail.com, [3] eaydin@ohu.edu.tr, [4] fatihcelik@ohu.edu.tr

ABSTRACT: One of the biggest problems encountered in many experimental studies is examining a real-size structure in the field or in a laboratory environment. With today's technological opportunities, it is possible to experimentally examine a real-sized structure in the field or in a laboratory environment. However, to do this, the manufacture of a large, real-size structure, experimental setup and measuring devices are required, which are costly. For this reason, it is not always possible to reach such a laboratory environment. It is very difficult to experimentally examine large-scale structures both economically and in terms of time saving. In this context, in this study, a scaling factor (λ) widely accepted in the literature was used to design a scaled model to represent a real-size structure. $\lambda=10$ was used in this scaling approach. A real-size three-story single-span steel prototype building was scaled to a laboratory-scale model structure and analyzed digitally with the Sap2000 program. The natural period/frequency values of the real-size prototype structure and the scaled model modeled in the Sap2000 program were examined. Later, Time history analyzes were performed using real earthquake records from El Centro (1940), Kobe (1995) and Northridge (1994). While real earthquake records were used as they were in the analysis of the prototype structure, these real earthquake records were used by scaling them depending on the scaling factor λ in the analysis of the scaled model. Subsequently, the digital analyzes of the prototype and scaled structure were compared by looking at the acceleration and displacement values of each floor. It was observed that the results were close to each other when scaled according to the scaling factor (λ). This situation demonstrated the accuracy of the scaling rates applied within the scope of the study. Thus, it has been shown that a real-size structure can be scaled to a model in a laboratory environment with correct scaling methods and that this prototype structure can be analyzed with more economical and simple methods.

Keywords: Prototype model, Structure ccaling, Seismic loads, Earthquakes, Time history analysis

1. INTRODUCTION

Within the scope of this study, although the studies presented in the literature related to scaling are generally on the structure-soil-pile interaction, scaling of the superstructure has also been done. Conducting a systematic study on scaling, Hokmabadi et al. [1] developed a scaling method in their study by taking into account all structure and ground-related parameters. This method, which pioneered many studies in the literature, made it possible to scale a prototype structure, ground or pile to represent the prototype structure, ground or pile in a laboratory environment. Meymand et al. [2] pointed out that, using this method, the natural frequency of the prototype should be scaled with an appropriate scaling relationship. It has been shown that by defining scaling conditions for density and acceleration, mass, length and time scale factors can be expressed in terms of the geometric scaling factor (λ) and a complete dimensional scaling relations can be derived for all variables examined.

Thejaswini et al. Experiments were carried out in a laboratory environment by scaling two five-storey and three-span buildings. Similarly, they scaled the model representing the prototype structure according to scaling laws. Shaking table tests of scale building models were carried out. The results obtained in

Comparison of Numerical Analysis of a Single-Span Steel Prototype Structure and a Scale Model
Structure Under the Effect of Seismic Loads

43

experimental and numerical studies have been compared [3,4]. They scaled the scaled model representing the 15-storey prototype building. They carried out single-axis shaking table tests of the superstructure model along with the ground model [5]. Shaking table experiments were carried out in a laboratory environment to better understand the dynamic behavior of a 10-storey scaled model representing a prototype structure. The scaling method was analyzed numerically and the period and frequency values obtained experimentally were compared. The values obtained from the results were found to be compatible and results close to the desired results were found according to the scaling method [6].

What is planned in this study is to scale the prototype structure and check whether the designed model structure's behavior in the digital environment is compatible. In addition, time history analysis under the influence of seismic loads was performed and the results obtained were checked with the scaling method and similar results were tried to be obtained. It will be a guide in terms of having the opportunity to observe the behavior of the planned prototype structure in advance and helping us determine the design criteria.

2. METHOD AND NUMERICAL ANALYSIS

2.1. Scaling Method

The purpose of using the scaling method is that it is not always possible to carry out real-scale experiments in terms of physical and infrastructure. Even if it were done, this would be very costly in economic terms. Instead of working at real scale, it is possible to reach an approximate conclusion by examining the laboratory experiments of the model structure, which is scaled with the λ scaling factor according to Table 1, which represents the prototype structure in the laboratory. In order to design the scaled model, the first step to be followed is to scale the model structures by taking into account the natural period/frequency, mass density, material properties and dimensions of the prototype structure, using the relations given in Table 1, with the help of scaling factors. While scaling within the scope of this study, the scaling factor was determined to be $\lambda=10$. This scale ratio was used to scale the parameters given in Table 1 below.

Table 1. Scaling relationships in terms of the geometric scaling factor (λ) [1]

Parameters	Scaling relationship
Mass density	1
Force	λ^3
Stiffness	λ^2
Modulus	λ
Acceleration	1
Shear-wave velocity	$\lambda^{1/2}$
Time	$\lambda^{1/2}$
Frequency	$\lambda^{-1/2}$
Length	λ
Stress	λ
Strain	1
EI	λ^5

2.2. Prototype Structure and Scaled Model

The features of the prototype structure and scaled model used in numerical analysis are given below. As can be clearly seen from Figure 1, the prototype building has three floors and a single span. The floor heights and floor spans of the steel prototype building are designed as 3 m. Material properties and cross-
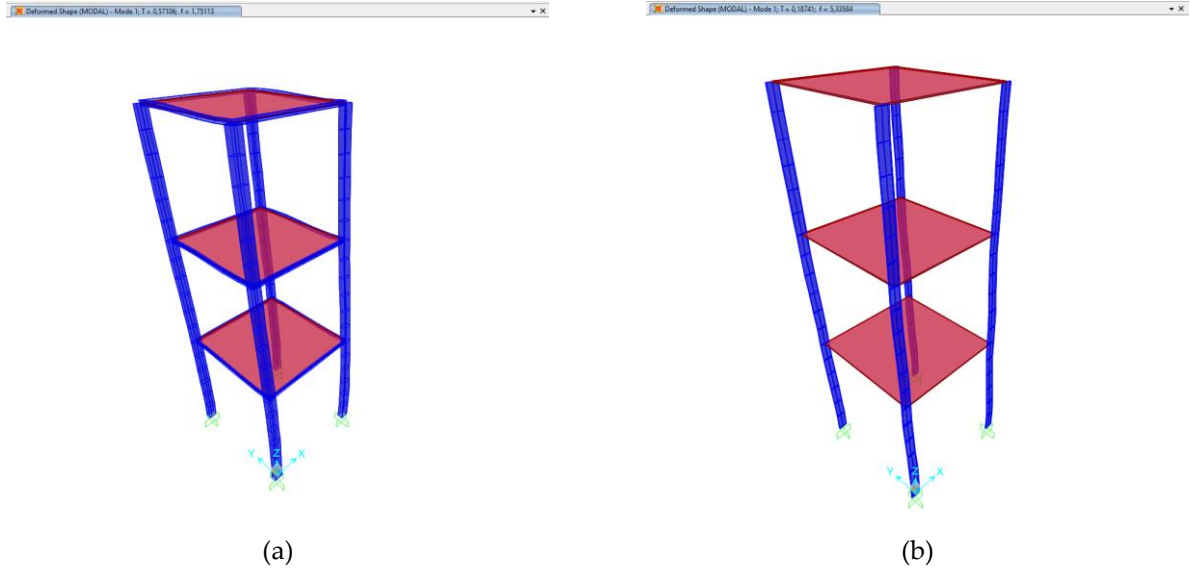
sections of the column, beam and floor of the prototype are shown in Table 2.
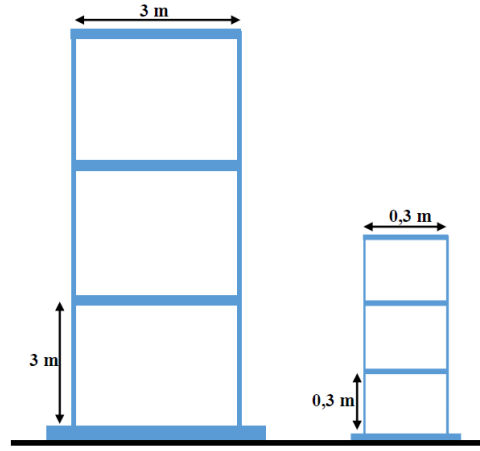
Figure 1. Designed prototype structure and scaled model

In scaling the prototype structure, which is a three-storey sliding frame, to the laboratory environment, the scaling ratio was chosen as $\lambda=10$. The parameters and their values that we will consider only in scaling the superstructure are given in Table 2 below. As can be clearly seen in Figure 1 above, the scaled building is scaled according to the prototype structure as a three-storey and single-span building. The floor heights and floor spans of the model building are determined as 0.3 m. The scaled model is designed as a steel structure. The material properties and cross-sections of the column and floor of the model building are shown in Table 2.

As can be seen in Figure 1, the prototype structure was first scaled by taking into account mass density, natural vibration frequency and geometric ratios. The mass densities of the prototype structure and model structure were kept constant as the scaling ratio was "1". Floor heights and floor openings were reduced by 10 times by λ. It is not correct to only do geometric scaling when scaling the column sections and material properties of the building. For the cross-sections and material elasticity modulus to be designed for the scaled model structure, the columns of the prototype structure must be scaled according to the flexural stiffness. From here, the column sections and material elasticity module of the model were determined. The flexural stiffness (EI) of the prototype was divided by λ^5 to obtain the flexural stiffness of the model structure depending on the geometric scaling factor (λ). Modal analyzes of the prototype and scaled model, whose column cross-sections and material properties were determined, were performed in the Sap2000 program. From these analyses, the natural vibration periods/frequencies of the structure were calculated. While the natural period of the prototype structure (T_n=0.57106 sec) was adjusted to be $\lambda^{1/2}$ times the natural period of the scaled model structure (T_n=0.18741 sec), the natural frequency of the prototype structure (f_n=1.75113 Hz) was adjusted to be $\lambda^{-1/2}$ times the natural frequency of the scaled model structure (f_n=5.33584 Hz). These period/frequency values were determined by trial and error using modal analysis in the Sap2000 program. Figure 2 shows the visuals of the structures whose modal analysis was performed in the Sap2000 program.

Comparison of Numerical Analysis of a Single-Span Steel Prototype Structure and a Scale Model
Structure Under the Effect of Seismic Loads

45

<center>(a)</center>

<center>(b)</center>

Figure 2. (a)Designed prototype structure; (b)Scaled model Modal analysis in Sap2000 program

The data of the prototype structure and the scaled structure are given in detail in Table 2 below. A model building design was made by scaling the created prototype structure. By analyzing the prototype and scaled model in the Sap2000 program, period/frequency values expressing the dynamic behaviors of the structures were also obtained.

<center>**Table 2.** Features of the prototype and model structure</center>

Parameters	Prototype structure		Model structure	
Number of floors	3		3	
Total height of the structure (m)	9		0.9	
Each floor height(m)	3		0.3	
Material type	Steel		Steel	
Material modulus of elasticity, E (MPa)	210000		210000	
Moment of inertia, I (m^4)	2.339 10^{-5}		2.25 10^{-10}	
Flexural stiffness of columns, EI (Nm^2)	4912.629		4.725 10^{-2}	
Column dimensions (m)	h	0.25	h	0.025
	b	0.15	b	0.003
	t	0.008		
Beam dimensions (m)	h	0.1		
	b	0.055		
	t_f	0.0057	-	
	t_w	0.0041		
Slab thickness (m)	0.03		0.003	
Natural period, T_n (sec)	0.57106		0.18741	
Natural frequency, f_n (Hz)	1.75113		5.33584	
Mass density, ρ (kg/m^3)	105.336		106.667	

Sap2000 analysis of the created prototype structure was performed. Using the scaling method, the same values of the scaled model were calculated, taking into account the mass density of the prototype structure, period/frequency and flexural stiffness of the columns. The mass density of the designed scaled model and the flexural stiffness of the columns were modeled in the Sap2000 program and natural period/frequency values were obtained by performing modal analysis. The parameters obtained from the

properties of the prototype structure according to the scaling method and the results obtained from the analysis of the scaled model are given in Table 3 below. When these values are compared, they are quite close to each other.

Table 3. Features of the prototype and model structure

Parameters	Prototype structure (Sap2000)	Model structure (Scaled)	Model structure (Sap2000)
Mass density, ρ (kg/m³)	105.336	105.336	106.667
Natural period, T_n (sec)	0.57106	0.18058	0.18741
Natural frequency, f_n (Hz)	1.75113	5.53756	5.33584
Flexural stiffness of columns, EI (Nm²)	4912.629	4.913×10^{-2}	4.725×10^{-2}

2.3. Scaling of earthquakes

Three real earthquake records were selected as the earthquake ground motion to be applied to the structure. El Centro (1940), Kobe (1995) and Northridge (1994) earthquake records were used. Some features of these earthquake records are seen in Table 4.

Table 4. Earthquake records and some reference features to be used in analysis
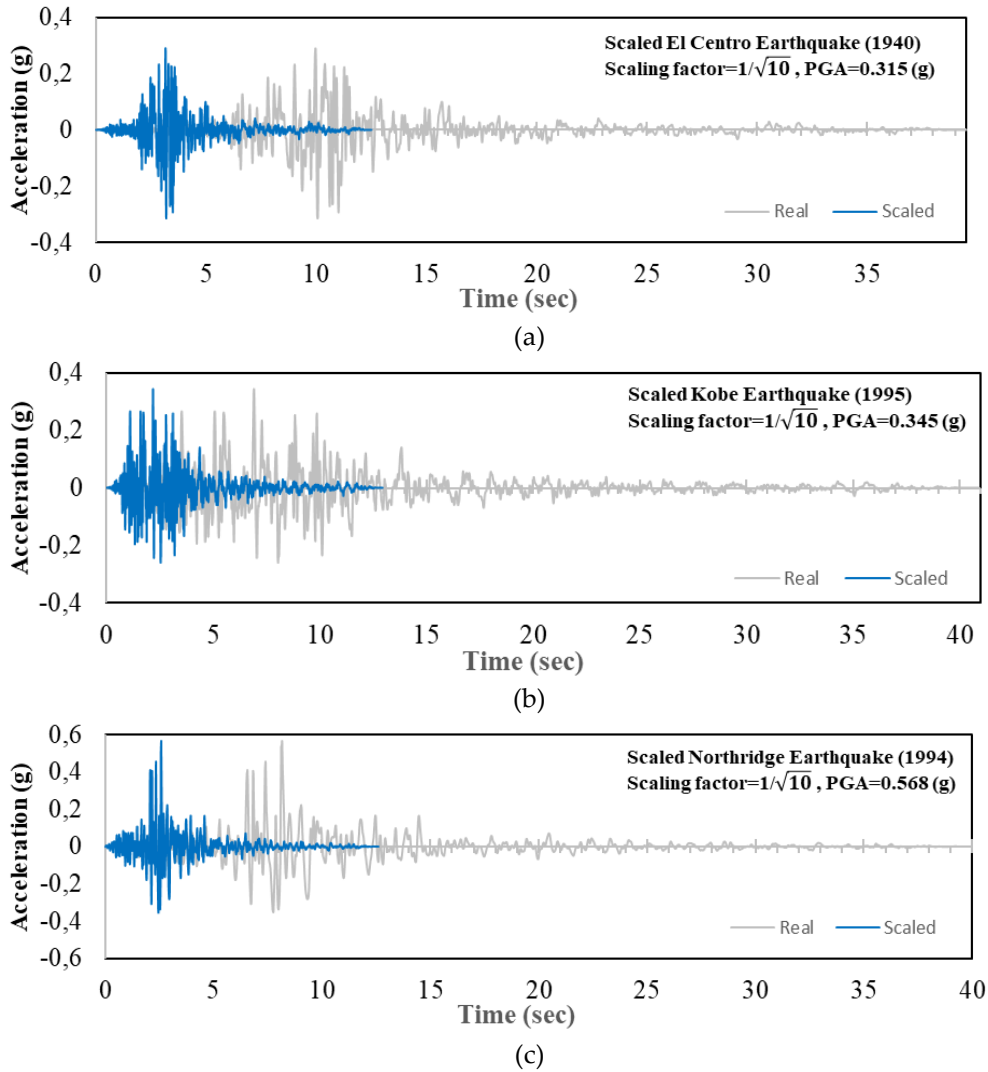
Earthquake	Country	Year	Peak ground acceleration (g)	Magnitude (Mw)	Duration (sec)
El Centro	ABD	1940	0.315	6.95	39.49
Kobe	Japonya	1995	0.345	6.9	40.9
Northridge	ABD	1994	0.568	6.69	39.89

Selected real earthquake records are based on Hokmabadi et al. [1] and was scaled to the laboratory environment using a systematic method. The purpose of using this scaling method is that it is not always possible to conduct real-scale experiments physically . Even if it were possible, it would be very costly in economic terms. Instead of working on a real scale, it is possible to reach an approximate conclusion by examining the experiments of the scaled model that represents the real structure in the laboratory. Likewise, real earthquake records must be scaled and applied to the model in the laboratory environment. Within the scope of the current study, real earthquake records were scaled by taking into account the scaling rates given in Table 1. When scaling in this study, the scaling factor was determined to be $\lambda=10$. While the acceleration values of the selected earthquakes remained the same, they were only scaled in time and these values were used.

In the figure above, real earthquake records with time-dependent acceleration values are scaled with the mentioned method. While real earthquake records were used in the Sap2000 analyzes of the prototype building, scaled earthquake records were used in the Sap2000 analyzes of the model building.

### 3. ANALYSIS RESULTS AND DISCUSSIONS

Time history analyzes of the prototype structure and the scaled model structure were made in the Sap2000 program. In these analyses, real and scaled earthquake ground motions given in Figure 3 above were used. As a result of numerical analysis, time-dependent displacement and acceleration values on each floor of the prototype and model are obtained graphically below.

Comparison of Numerical Analysis of a Single-Span Steel Prototype Structure and a Scale Model
Structure Under the Effect of Seismic Loads

47

Figure 3. Real and scaled (a) El Centro earthquake; (b) Kobe earthquake; (c) Northridge earthquake

Figure 4 below shows the displacement values at each floor of the real prototype building and the scaled model under the influence of the real and scaled El Centro (1940), Kobe (1995) and Northridge (1994) earthquakes, respectively. If each displacement value on the same floor is scaled by dividing by $\lambda=10$ according to the geometric scaling factor by looking at the parameter in Table 1, it can be seen that these are acceptable values.

As in the displacement graphs, Figure 5 below shows the acceleration values at each floor of the real prototype building and the scaled model under the influence of the real and scaled El Centro (1940), Kobe (1995) and Northridge (1994) earthquakes, respectively. These values are considered as "1" in the scaling method. In other words, the acceleration values of the same floors of the prototype and the model must be the same. The results obtained here show that if the acceleration values on the same floors are scaled, they are acceptable values.
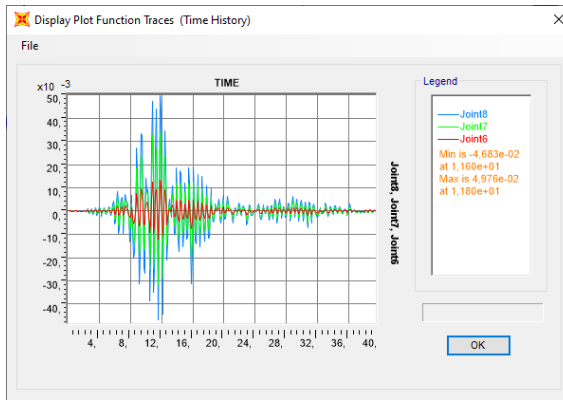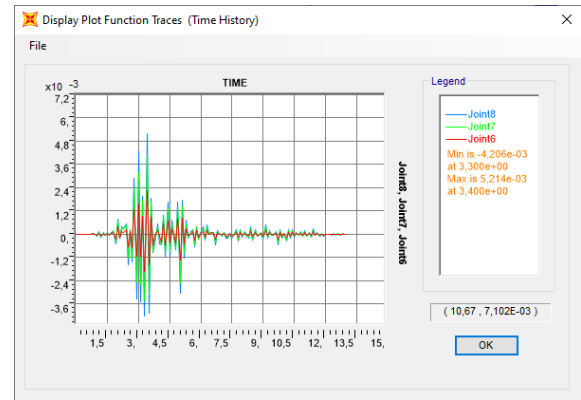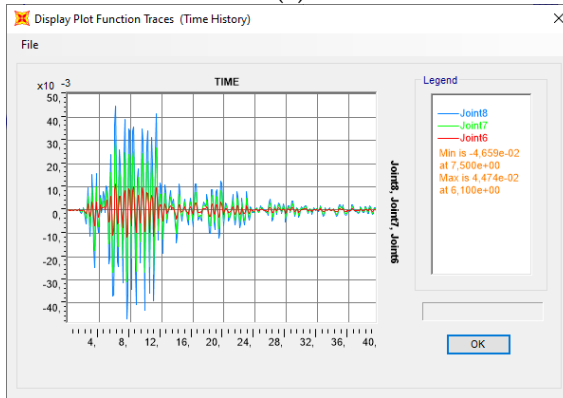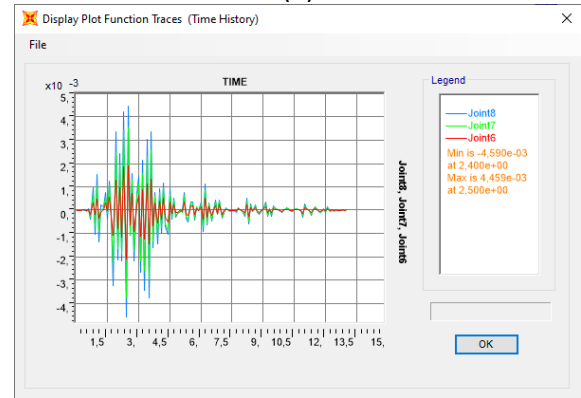
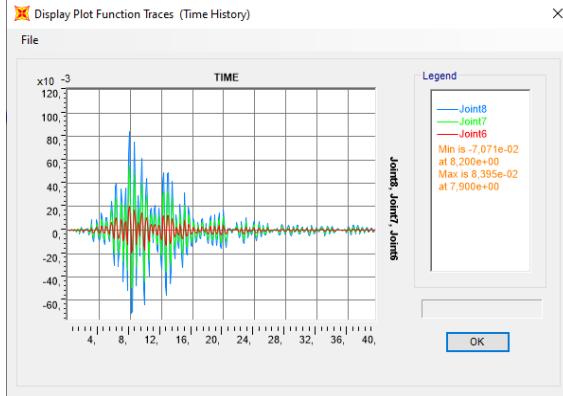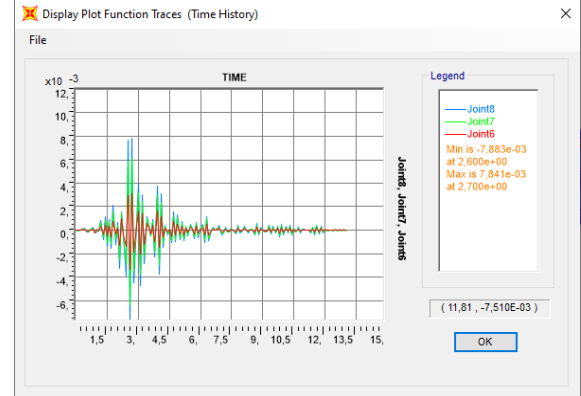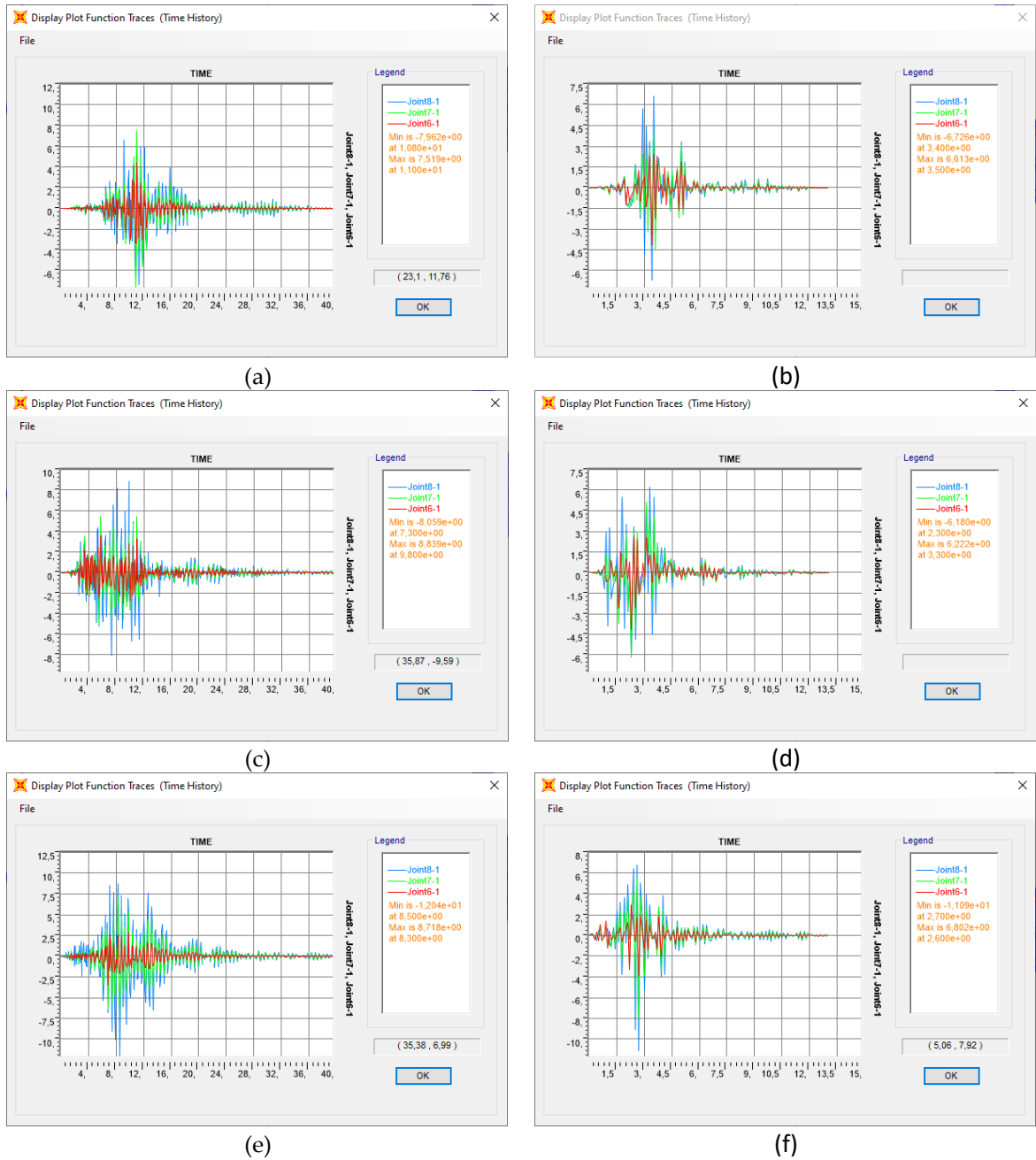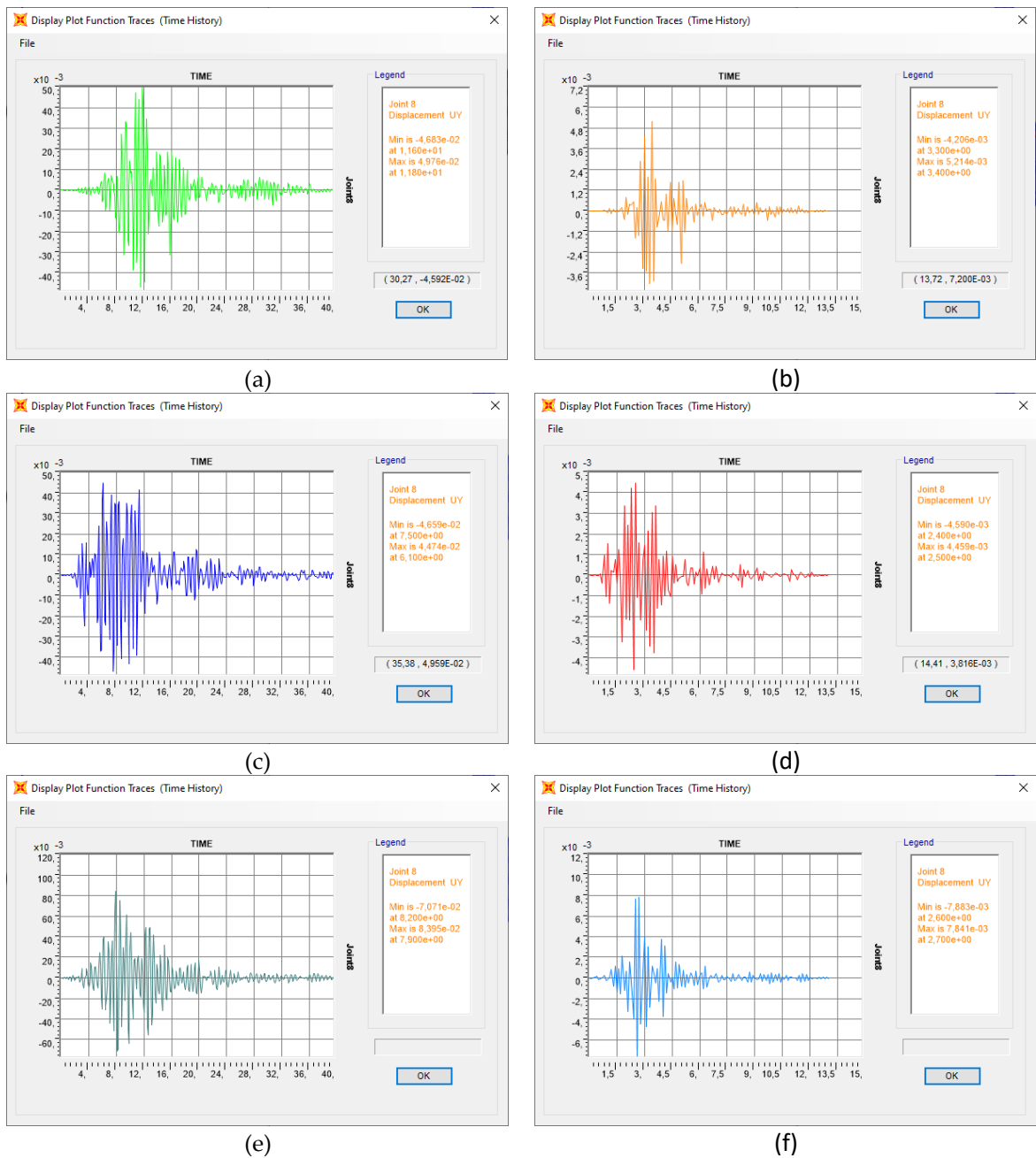**Figure 4.** Time-dependent displacement values of each floor of the prototype and model structure, respectively, under the influence of the following earthquakes: (a,b) El Centro (1940); (c,d) Kobe (1995); (e,f) Northridge (1994)
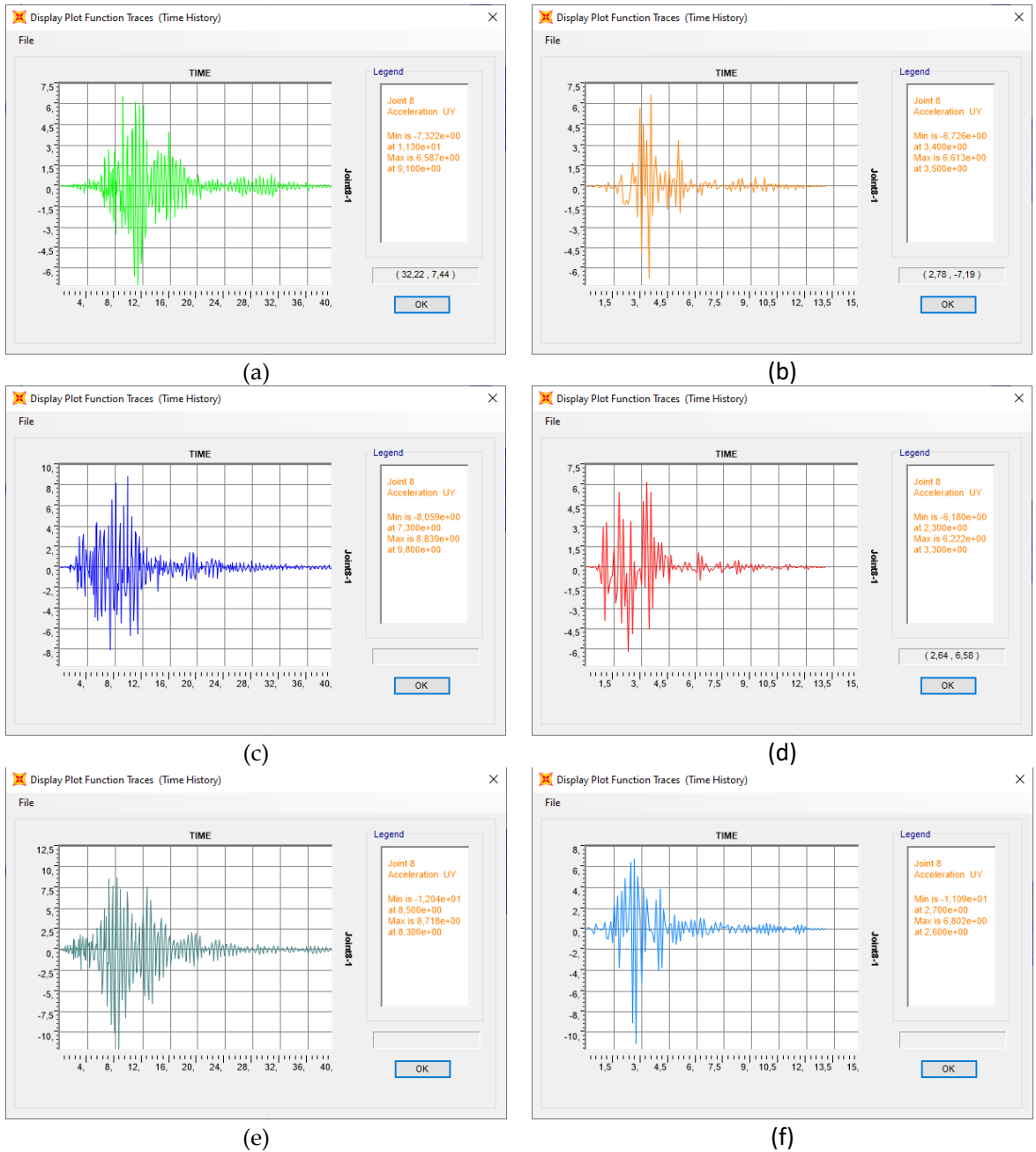
Figure 5. Time-dependent acceleration values of each floor of the prototype and model structure, respectively, under the influence of the following earthquakes: (a,b) El Centro (1940); (c,d) Kobe (1995); (e,f) Northridge (1994)

Generally, the most dominant mode in structures is the first mode. In other words, it is the situation where the top floor experiences peak displacement. As a result of the time history analysis obtained, the displacement and acceleration values on the top floor of the prototype and model building will be examined and when these results are compared according to the scaling method, very close results are obtained. Figures 6 and 7 below show the time-dependent displacement and acceleration values at the top floor of the prototype and model building under the influence of three earthquakes, respectively. When these displacement and acceleration values are scaled and compared, the results are quite close.

(a)

(b)

(c)

(d)

(e)

(f)

Figure 6. Time-dependent displacement values of the top floor of the prototype and model structure, respectively, under the influence of the following earthquakes: (a,b) El Centro (1940); (c,d) Kobe (1995); (e,f) Northridge (1994)

Comparison of Numerical Analysis of a Single-Span Steel Prototype Structure and a Scale Model
Structure Under the Effect of Seismic Loads

**51**

(a)

(b)

(c)

(d)

(e)

(f)

Figure 7. Time-dependent acceleration values of the top floor of the prototype and model
structure, respectively, under the influence of the following earthquakes: (a,b) El Centro (1940);
(c,d) Kobe (1995); (e,f) Northridge (1994)

In Figures 8-10 below, the peak displacement and acceleration values of each floor of the earthquakes used in time history analyzes for the prototype and model building are given respectively. When the displacement and acceleration values are scaled according to the scaling method based on the geometric scaling factor, it is seen that the results are quite close to each other.
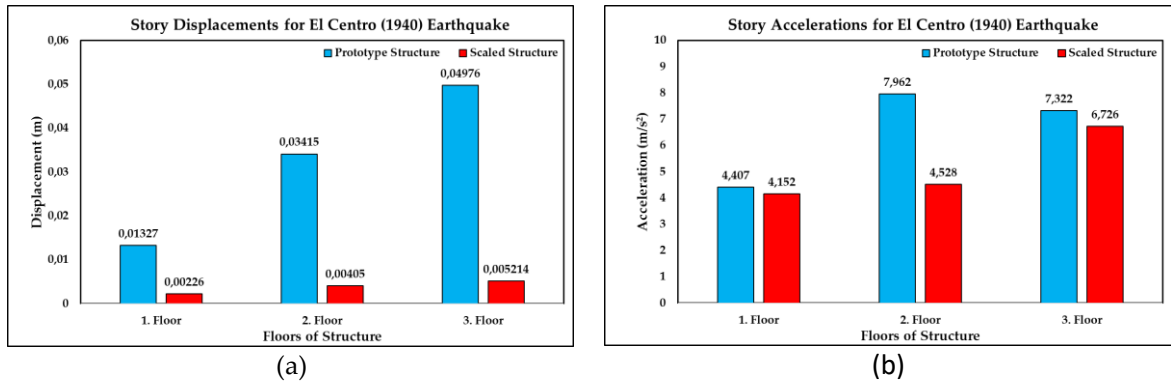
Figure 8. (a) Displacement; (b) Acceleration; of each floor of the prototype and model structure under the influence of the Kobe (1995) earthquake
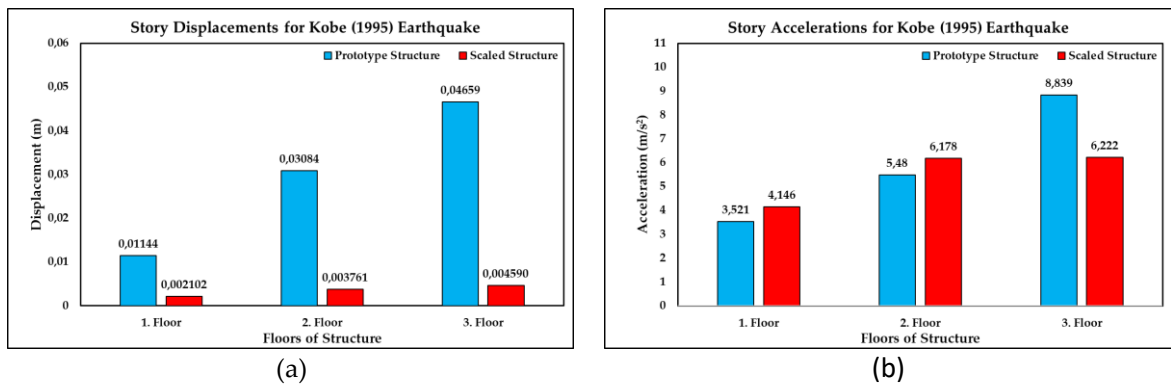
Figure 9. (a) Displacement; (b) Acceleration; of each floor of the prototype and model structure under the influence of the El Centro (1940) earthquake
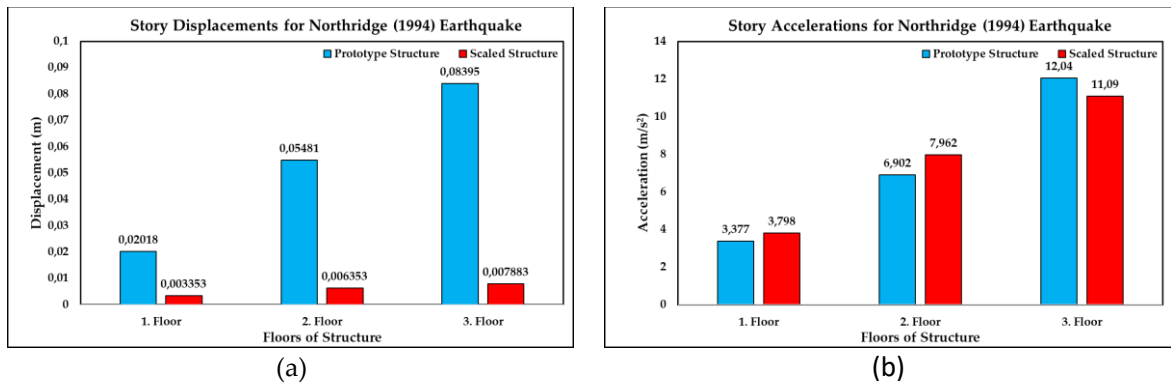
Figure 10. (a) Displacement; (b) Acceleration; of each floor of the prototype and model structure under the influence of the Northridge (1994) earthquake

Parameters such as displacement and acceleration values of each floor of the building give us an idea about how the structure behaves. As can be clearly seen from the displacement and acceleration graphs of each floor above, it can be said that the behaviors of the prototypes and models are similar, although the characteristics of the earthquakes used in the numerical analyzes are different. This shows that the scaling method is quite successful.

4. CONCLUSIONS

The aim of this study is to create a model structure by accurately scaling a prototype structure and to examine the behavior of these two structures under the influence of seismic loads. First, a prototype

structure was created in the digital environment and the model structure was obtained by scaling the created prototype. A superstructure was scaled by taking into account the scaling parameters so that it could be used experimentally in the laboratory environment. In this scaling, the mass density of the prototype (ϱ=105.336 kg/m^3) and the mass density of the scaled model (ϱ=106.667 kg/m^3) were very close to each other, as seen from the results obtained. When scaling the columns of the prototype building, it is not correct to only do geometric scaling. Here, along with the rigidity of the columns, the elastic modulus of the material is also important. These two parameters express the flexural stiffness (EI) and the design must be made accordingly. It is aimed to obtain the flexural stiffness of the model structure, EI=4.913 10^{-2} Nm^2, by dividing the flexural stiffness of the prototype structure, EI=4912.629 Nm^2, by λ^5, depending on the geometric scaling factor (λ). The flexural stiffness of the scaled model was found to be EI=4.725 10^{-2} Nm^2 and was very close to the value found by the scaling method. According to the data obtained, the prototype and scaled model were modeled in the Sap2000 program and modal analyzes were performed. As a result of the analyses, the natural period and frequency values of the prototype structure were found to be T_n=0.57106 sec and f_n=1.75113 Hz. By dividing the natural period of the prototype structure by $\lambda^{1/2}$ and its natural frequency by $\lambda^{-1/2}$ with the scaling method, it is aimed to find the natural period and frequency values of the model as T_n=0.18058 sec and f_n=5.53756 Hz. The results obtained from the digital analysis of the scaled model Natural period and frequency values were obtained as T_n=0.18741 sec and f_n=5.33584 Hz. By looking at these parameters, it was concluded that the scaled model would successfully represent the prototype structure.

Afterwards, the displacement and acceleration values of the prototype and scaled model structure under the influence of dynamic loads were examined. The values of these parameters, which express the dynamic behavior of the building, on all floors and on the top floor, where the first mode of the building is dominant, were examined and compared according to the scaling method. In this comparison, it was aimed to find the displacement values corresponding to that floor of the model building by dividing the displacement values of the floors of the prototype by the scaling factor λ. Similarly, with the scaling method, it is aimed to find the acceleration values of the floors of the prototype equal to the acceleration values corresponding to that floor of the model building. According to the results of the displacement and acceleration graphs obtained, although these displacement and acceleration values did not approach our target values on some floors, in most cases they were quite close. As a result, this study shows that the dynamic behaviors of a scaled prototype and a scaled model are compatible in digital analysis. According to the results obtained, it has been observed that when a prototype structure is scaled correctly, this scaled model will represent a prototype structure in the digital environment. This study was carried out using only digital analysis and three real earthquake records. However, it is planned to use more real earthquake records with different characteristics in future studies and to compare the scaled model with shaking table experiments in a laboratory environment with numerical analyses.

Declaration of Ethical Standards

Declaration of Competing Interest

Funding / Acknowledgements

REFERENCES

[1]   A. S. Hokmabadi, B. Fatahi, and B. Samali, "Physical modeling of seismic soil-pile-structure interaction for buildings on soft soils," *International Journal of Geomechanics,* vol. 15, no. 2, Apr., pp. 1-18, 2014.

[2]   P. J. Meymand, "Shaking table scale model tests of nonlinear soil-pile superstructure interaction in soft clay," Doctoral dissertation, University of California, Berkeley, 1998.

[3]   R. M. Thejaswini, "Effect of Subsoil on the Seismic Response of the Setback Buildings," In Proc. Indian Geotechnical Conference '19, 2021, pp. 687-695.

[4]   R. M. Thejaswini, L. Govindaraju, and V. Devaraj, "Experimental and numerical studies on setback buildings considering the SSI effect under seismic response," *Civil Engineering Journal,* vol. 7, no. 3, Mar., pp. 431-448, 2021.

[5]   H. R. Tabatabaiefar, B. Fatahi, K. Ghabraie, and W. H. Zhou, "Evaluation of numerical procedures to determine seismic response of structures under influence of soil-structure interaction," *Structural Engineering and Mechanics,* vol. 56, no. 1, Sep., pp. 27-47, 2015.

[6]   K. G. Subramanya, L. Govindaraju and R. Ramesh Babu, "Experimental Studies on the Dynamic Response of Buildings Supported on Pile and Piled Raft Foundation in Soft Clay," in *Earthquake Engineering and Disaster Mitigation*, R. S. Jakka, Y. Singh, T. G. Sitharam and B. K. Maheshwari, Eds. Singapore: Springer Nature, 2023, pp. 219-239.